Upregulated stromal EGFR and vascular remodeling in mouse xenograft models of angiogenesis inhibitor–resistant human lung adenocarcinoma

Tina Cascone,[1,2] Matthew H. Herynk,[1] Li Xu,[1] Zhiqiang Du,[1] Humam Kadara,[1] Monique B. Nilsson,[1] Carol J. Oborn,[3] Yun-Yong Park,[4] Baruch Erez,[1] Jörg J. Jacoby,[1] Ju-Seog Lee,[4] Heather Y. Lin,[5] Fortunato Ciardiello,[2] Roy S. Herbst,[1] Robert R. Langley,[3] and John V. Heymach[1,5]

[1]Department of Thoracic/Head and Neck Medical Oncology, University of Texas M.D. Anderson Cancer Center, Houston, Texas, USA.
[2]Division of Medical Oncology, "F. Magrassi — A. Lanzara" Department of Clinical and Experimental Medicine, Second University of Naples, Naples, Italy.
[3]Department of Cancer Biology, [4]Department of Systems Biology, and [5]Department of Biostatistics, University of Texas M.D. Anderson Cancer Center, Houston, Texas, USA.

Angiogenesis is critical for tumor growth and metastasis, and several inhibitors of angiogenesis are currently in clinical use for the treatment of cancer. However, not all patients benefit from antiangiogenic therapy, and those tumors that initially respond to treatment ultimately become resistant. The mechanisms underlying this, and the relative contributions of tumor cells and stroma to resistance, are not completely understood. Here, using species-specific profiling of mouse xenograft models of human lung adenocarcinoma, we have shown that gene expression changes associated with acquired resistance to the VEGF inhibitor bevacizumab occurred predominantly in stromal and not tumor cells. In particular, components of the EGFR and FGFR pathways were upregulated in stroma, but not in tumor cells. Increased activated EGFR was detected on pericytes of xenografts that acquired resistance and on endothelium of tumors with relative primary resistance. Acquired resistance was associated with a pattern of pericyte-covered, normalized revascularization, whereas tortuous, uncovered vessels were observed in relative primary resistance. Importantly, dual targeting of the VEGF and EGFR pathways reduced pericyte coverage and increased progression-free survival. These findings demonstrated that alterations in tumor stromal pathways, including the EGFR and FGFR pathways, are associated with, and may contribute to, resistance to VEGF inhibitors and that targeting these pathways may improve therapeutic efficacy. Understanding stromal signaling may be critical for developing biomarkers for angiogenesis inhibitors and improving combination regimens.

Introduction

Tumor growth and metastasis are dependent on the formation of a vascular supply, i.e., angiogenesis (1–3). Most therapeutic efforts directed toward inhibiting the angiogenic process for the treatment of cancer have focused on the VEGF pathway (4–8). The majority of the mitogenic, angiogenic, and permeability-enhancing properties of VEGF are mediated by VEGF receptor–2 (VEGFR2) (8). Several inhibitors of this pathway have received FDA approval and are currently in clinical use; these include bevacizumab (BV; Avastin; Genentech), a monoclonal antibody that blocks human VEGF (9, 10), and small-molecule inhibitors of the VEGFR2 tyrosine kinase (e.g., sorafenib, sunitinib, and pazopanib) (11). The results from phase III clinical trials demonstrated that the addition of BV to standard therapy prolongs progression-free survival (PFS) and/or overall survival, and improves objective tumor responses, in patients with advanced malignancies including non–small-cell lung cancer (NSCLC) and colon cancer (12, 13). However, not all patients benefit from antiangiogenic therapy, and those tumors that initially respond to treatment will ultimately become refractory and relapse (14, 15). Therefore, the development of more durable cancer therapies requires an improved understanding of the cellular and molecular mechanisms that mediate resistance to antiangiogenic agents.

Recent studies suggest that blockade of the VEGFR2 signaling pathway may prompt some tumors to increase their expression of secondary molecules in order to sustain the neovascularization response (16). Casanovas et al. reported that although anti-VEGFR therapy initially blocks new blood vessel formation and tumor growth in a transgenic model of pancreatic islet cell tumors, both angiogenesis and tumor progression are eventually restored by the increased synthesis of other angiogenic factors from tumor cells (17). There is also evidence suggesting that commonly occurring genetic alterations in tumor cells may uncouple tumor dependency on a vascular blood supply. For example, loss of *p53* enhances the ability of tumor cells to withstand hypoxic conditions (18), which renders p*53*-deficient tumors to be at least partially resistant to antiangiogenic therapy (19). Other tumor cells have been shown to alter their pattern of growth when challenged with antiangiogenic therapy. Instead of recruiting resident ECs to form new vascular networks, these tumor cells meet their metabolic requirements by residing in close proximity to preexisting blood vessels (20). Incomplete target inhibition after treatment with VEGFR antago-

Conflict of interest: J.V. Heymach and R.S. Herbst have served on advisory boards for Genentech and AstraZeneca and receive research support from AstraZeneca.

Citation for this article: *J Clin Invest.* 2011;121(4):1313–1328. doi:10.1172/JCI42405.

nists has been described in orthotopic models of pancreatic cancer, as well as in patients with this type of cancer and with advanced soft tissue sarcomas (21, 22).

Emerging evidence suggests that stromal cells may also play an important role in mediating resistance to antiangiogenic therapies. Shojaei et al. reported that localization of Gr-1$^+$CD11b$^+$ myeloid cells to various murine tumors rendered the neoplasms refractory to anti-VEGF therapy (23). Myeloid cells provide a rich reserve of angiogenic molecules and possess potent immunosuppressive activity (24), both of which favor tumor progression. Similarly, a recent study evaluating the effects of a neutralizing VEGF antibody in murine lymphoma models demonstrated that tumor-associated fibroblasts upregulate expression of PDGF-C when the VEGFR pathway is blocked, ensuring the continued formation of tumor blood vessels when signaling through this pathway is prohibited (25). Together, these studies provide evidence that both tumor cells and stromal cells contribute to VEGF inhibitor resistance, although their respective contributions remain incompletely characterized and are likely to vary based on molecular features of the tumor and its microenvironment.

We hypothesized that there may be additional stromal and tumor cell mechanisms that contribute to the resistant phenotype. To assess this question, we investigated 3 different models with varying de novo responsiveness to BV. In order to discriminate between tumor (human) and stromal (mouse) genes that may be associated with acquired resistance to BV, we performed species-specific gene expression profiling using vehicle-treated (controls) and BV-resistant xenografts. This approach demonstrated that gene expression changes associated with resistance occurred primarily in stromal cells, highlighted different modes of vascular remodeling that may accompany the emergence of resistance, and led to the identification of what we believe to be a previously unrecognized mechanism for acquired resistance to BV involving upregulation of EGFR signaling in vascular pericytes.

Results

NSCLC xenografts exhibit different patterns of resistance to BV. To investigate the mechanisms by which NSCLC xenografts develop resistance to VEGF blockade, we initially injected male nude mice with either H1975 or A549 human NSCLC adenocarcinoma cells. These models were selected because in prior studies, we observed that A549 xenograft tumors were relatively insensitive to VEGF inhibitors de novo (relative primary resistance), whereas H1975 tumors were more initially responsive to these agents, experiencing significant tumor volume reduction typically lasting more than 1 month (26). Furthermore, the tumor cells contain 2 common alterations associated with EGFR tyrosine kinase inhibitor (TKI) resistance: a T790M EGFR mutation (H1975 model; ref. 27) and a KRas mutation (A549 model; ref. 28). Approximately 3 weeks after tumor cell injection, mice bearing tumors with a mean volume of approximately 270 mm^3 were randomized to receive either vehicle control or BV (see Methods). Animals were treated for 2 weeks (short-term treatment) or until they were euthanized due to tumor burden. Tumors were considered to be resistant when they tripled in volume (i.e., tumor progression) compared with the pretreatment tumor size, and PFS was measured as the time from initiation of treatment until tumor progression. In H1975 tumors, as assessed by tumor volume change ratio ($\Delta T/\Delta C$; see Methods), short-term treatment with BV inhibited tumor growth by 77% compared with vehicle-treated control tumors ($\Delta T/\Delta C$ 23.1%; P = 0.015, Mann Whitney test; Figure 1, A and C). In A549 xenografts, in contrast, a nonsignificant 16% reduction in tumor growth was observed ($\Delta T/\Delta C$ 83.8%; P = 0.381, Mann Whitney test; Figure 1, B and C).The individual tumor growth curves shown in Figure 1, D and E, illustrate the growth kinetics of H1975 and A549 xenografts treated with vehicle or BV for a longer period until progression. All H1975 control xenografts progressed within 31 days of treatment onset, with median PFS of 6 days. In contrast, 67% of xenografts (4 of 6) receiving BV developed resistance, and the median PFS was 138 days (P = 0.0007, log-rank test; Figure 1D). A549 tumors were less responsive to BV and had a median PFS of 40 days compared with 29.5 days in control tumors (P = 0.390, log-rank test; Figure 1E). These results showed that H1975 tumors were initially responsive to BV therapy, but eventually acquired resistance after prolonged treatment with the drug, whereas A549 tumors demonstrated relative primary resistance to BV.

Acquired resistance to BV is associated with sustained inhibition of VEGFR2 activation and reduced endothelial apoptosis. To determine whether acquired resistance to BV is the result of increased VEGFR2 signaling, potentially through increased expression of murine VEGF or another mechanism to bypass blockade of human VEGF by this agent, we evaluated the phosphorylation status of VEGFR2 in control-treated (vehicle progression), BV-sensitive (2 weeks BV treatment), and BV-resistant (BV progression) tumors using immunofluorescence (IF) staining. In control tumors, phosphorylated VEGFR2 (p-VEGFR2) was readily detected on CD31$^+$ tumor-associated ECs. However, no p-VEGFR2 was detected on the vasculature of BV-sensitive tumors or the BV progression group (Supplemental Figure 1A; supplemental material available online with this article; doi:10.1172/JCI42405DS1). To evaluate changes in stromal (defined here as nontumor cells derived from the host) and tumor-derived VEGF in H1975 BV-resistant tumors, we quantified mouse *Vegfa* and human *VEGFA* mRNA expression by quantitative real-time PCR (qRT-PCR). We observed no change in mouse *Vegfa* mRNA expression in resistant xenografts, whereas human *VEGFA* mRNA levels were increased in resistant tumors, compared with controls ($P < 0.05$; Supplemental Figure 1B). Despite the increase in VEGF ligand, however, VEGFR2 phosphorylation remained suppressed in BV-resistant tumors.

We then assessed whether the acquisition of resistance was associated with changes in endothelial apoptosis. We performed double IF staining for CD31$^+$ and TUNEL$^+$ cells in H1975 tumors following short-term BV treatment and BV progression and determined the percentage of apoptotic ECs (CD31$^+$TUNEL$^+$; Supplemental Figure 1, C and D). The percentage of apoptotic ECs significantly increased following 2 weeks of BV treatment compared with control xenografts ($P < 0.05$). However, at the time of progression, EC apoptosis diminished significantly ($P < 0.05$ versus short-term BV), to levels comparable to those of vehicle-treated tumors. Thus, EC apoptosis increased while tumors were initially responding to VEGF signaling blockade and returned to levels comparable to those of controls in tumors that acquired BV resistance.

In the same tumors, we also quantified the percentage of total apoptotic cells using laser scanning cytometry (LSC; data not shown). Tumors sensitive to BV showed an increased percentage of total TUNEL$^+$ cells compared with controls (2 weeks vehicle treatment), whereas no significant changes were observed in BV-resistant tumors compared with controls (vehicle progression).

Stromal and tumor cell gene expression changes in H1975 BV-resistant xenografts. To identify changes in stromal and tumor gene expres-

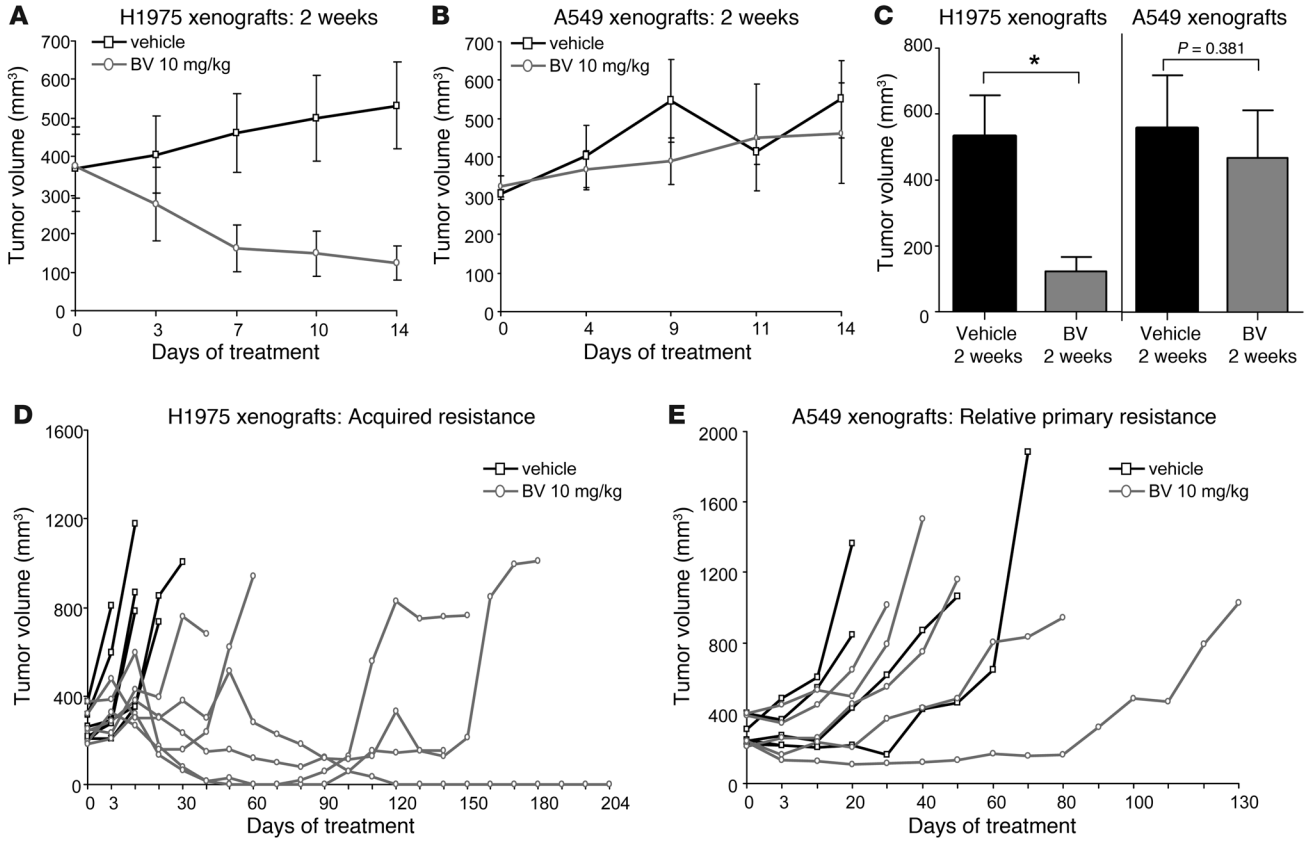

Figure 1

H1975 and A549 NSCLC xenografts show different patterns of resistance to BV treatment. (**A** and **B**) Tumor growth curves of H1975 (**A**; $n = 5$ per group) and A549 (**B**; $n = 6$ per group) xenografts receiving vehicle (control) and BV for 2 weeks. (**C**) Mean tumor volume obtained at the last measurement in H1975 and A549 xenografts treated with BV for 2 weeks compared with controls ($\Delta T/\Delta C$). *$P < 0.05$, Mann-Whitney test. (**D** and **E**) Individual tumor growth curves of H1975 (**D**; $n = 6$ per group) and A549 (**E**; $n = 5$ per group) xenografts treated with vehicle and BV until animals became moribund. Tumors were considered resistant (progression) when tripled in volume compared with the beginning of the treatment.

sion associated with acquired resistance to anti-VEGF therapy, we performed RNA microarray analyses comparing H1975 control and BV-resistant xenografts ($n = 3$ per group) using Illumina mouse-specific (WG-6 v2) and human-specific (WG-6 v3) expression arrays. Probes in these arrays have been designed to minimize cross-species reactivity; consistent with this, essentially no cross-reactivity was observed in experiments mixing human and mouse cell lines (E.S. Park, unpublished observations). We found that a much larger number of stromal mouse genes were significantly modulated in BV progression versus control vehicle progression xenografts compared with human tumor genes (1,385 stromal genes versus 98 tumor genes), according to the statistical criteria described in Methods. We observed significant changes in the expression of genes involved in angiogenesis, lymphangiogenesis, and hypoxia signaling pathway between BV-resistant and control xenografts. Both *Egfr* and *Fgfr2* genes were upregulated in the stromal compartment, but not in tumor cells, of H1975 BV-resistant tumors compared with controls, as well as stromal molecules and ligands associated with these signaling pathways (e.g., *Epgn*, *Areg*, *Fgf13*, and *Fgfbp1*; Figure 2A and Supplemental Table 1). Among human angiogenic or hypoxia-regulated genes, carbonic anhydrase IX (*CA9*) was significantly upregulated in BV-resistant tumors (Figure 2A and Supplemental Table 2).

We next sought to identify pathways potentially important in the acquired resistance phenotype. Functional gene-interaction network analyses of gene features differentially expressed between the mouse stroma of BV-resistant and vehicle-treated H1975 xenografts, using Ingenuity Pathway Analysis, revealed significant modulation in the predicted function of a gene neighborhood and interaction network surrounding *Egfr*, based on the number of focus genes and nodes of interaction ($P < 0.001$; Figure 2B). In addition, the modulated gene network associated with *Egfr* expression included downregulated proapoptotic genes, such as the Bcl-2 family member protein *Bax* and apoptotic peptidase activating factor 1 (*Apaf1*). Genes with prosurvival functions, such as the heat shock protein *Dnajb1*, were upregulated.

Next, to validate the changes in expression of the significantly modulated network-hub gene *Egfr*, we assessed the human and mouse mRNA levels using qRT-PCR. Consistent with the microarray data, we observed a 2.5-fold increase in mouse *Egfr* mRNA levels in H1975 BV-resistant xenografts compared with controls ($P < 0.05$; Figure 2C). Human *EGFR* mRNA levels were not significantly different than those of controls. We also validated the stromal expression of *Fgfr2*, which we noted to be upregulated in BV-resistant H1975 tumors in the microarray analysis. A significant increase in mouse *Fgfr2*, but not human *FGFR2*, mRNA

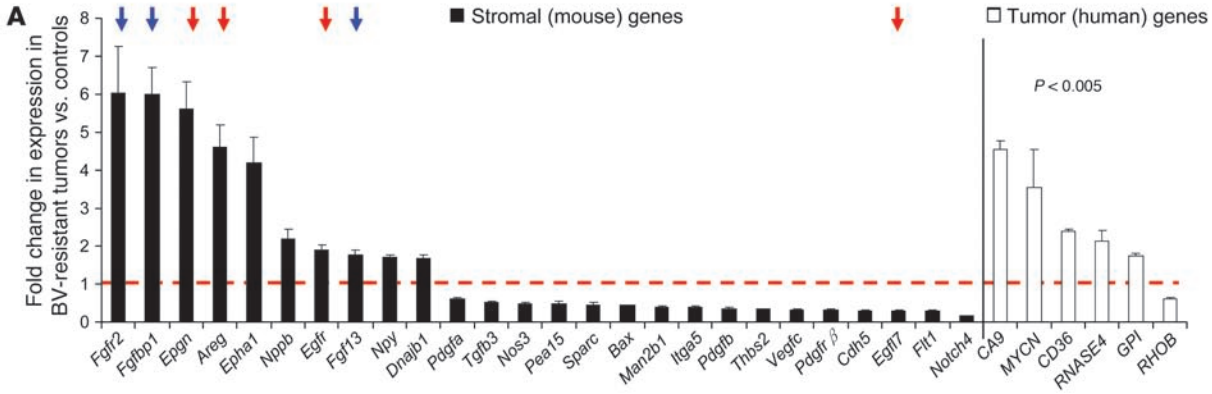
A
Fold change in expression in BV-resistant tumors vs. controls
Stromal (mouse) genes
Tumor (human) genes
P < 0.005
Fgfr2
Fgfbp1
Epgn
Areg
Epha1
Nppb
Egfr
Fgfr13
Npy
Dnajb1
Pdgfa
Tgfb3
Nos3
Pea15
Sparc
Bax
Man2b1
Itga5
Pdgfb
Thbs2
Vegfc
Pdgfr β
Cdh5
Egfl7
Flt1
Notch4
CA9
MYCN
CD36
RNASE4
GPI
RHOB

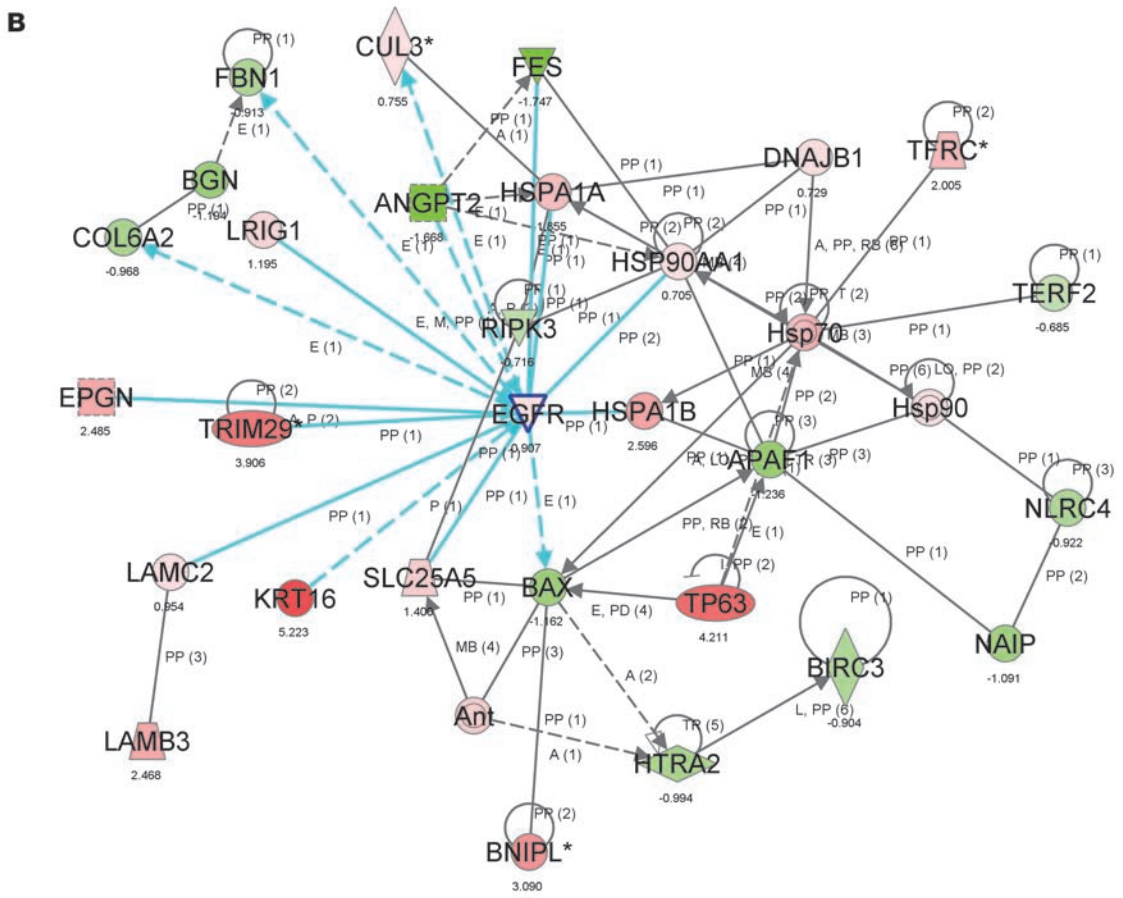
B
FBN1
CUL3*
FES
DNAJB1
TFRC*
BGN
ANGPT2
HSPA1A
COL6A2
LRIG1
HSP90AA1
TERF2
RIPK3
Hsp70
EPGN
TRIM29*
EGFR
HSPA1B
Hsp90
APAF1
NLRC4
LAMC2
KRT16
SLC25A5
BAX
TP63
NAIP
BIRC3
Ant
LAMB3
HTRA2
BNIPL*

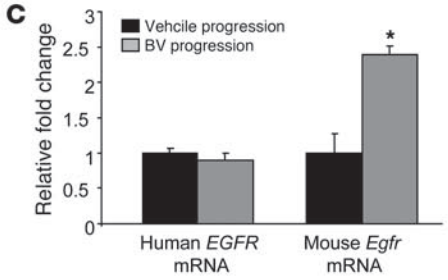
C
Vehicle progression
BV progression
Relative fold change
Human EGFR mRNA
Mouse Egfr mRNA

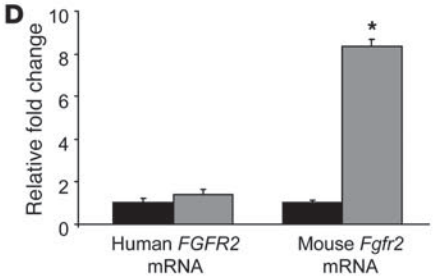
D
Relative fold change
Human FGFR2 mRNA
Mouse Fgfr2 mRNA

Figure 2
BV resistance is associated with increased expression of stromal genes involved in angiogenesis. (**A**) Stromal and human angiogenic genes were differentially regulated in H1975 BV-resistant xenografts compared with vehicle controls ($n = 3$ per group). $P < 0.005$, 2-sample *t* test with random variance model. Exact permutation *P* values for significant genes were computed based on 10 available permutations. Data represent differences in fold change of genes in BV-resistant tumors versus controls. The dashed red line indicates fold change 1 (i.e., no change versus controls). Red and blue arrows indicate *Egfr* and *Fgfr* family member genes, respectively. (**B**) Functional pathway analysis of selected genes and their interaction nodes in a gene network significantly modulated between the BV-resistant and control xenograft mouse stroma. Network score was calculated by the inverse log of the *P* value and indicates the likelihood of focus genes in a network being found together not by chance. The selected genes (*Egfr*, *Bax*, and *Dnajb1*) and their interaction segments are highlighted by a blue border. Gene expression variation by at least 1.5-fold is indicated by color (red, upregulated; green, downregulated; gray, NS). (**C** and **D**) qRT-PCR showing human *EGFR* and mouse *Egfr* (**C**) and human *FGFR2* and mouse *Fgfr2* (**D**) mRNA expression in H1975 xenografts that progressed on vehicle and BV treatments ($n = 4$ per group). Data are normalized relative to vehicle progression samples and shown as relative fold change. $^*P < 0.05$, *t* test.

expression was observed in H1975 BV-resistant xenografts compared with controls ($P < 0.05$; Figure 2D).

EGFR is activated on stromal cells of H1975 and A549 BV-resistant tumors. Given our observation that mouse *Egfr* mRNA was increased in BV-resistant tumors, we next evaluated EGFR protein expression in H1975 tumors by IF staining using antibodies directed against CD31 and EGFR (Supplemental Figure 2A). Quantification of EGFR staining by LSC analysis revealed that prolonged administration of BV produced a nearly 10-fold increase in the number of EGFR-expressing cells in H1975 BV-resistant tumors compared with control tumors ($P < 0.01$; Figure 3A and Supplemental Figure 2A). We also evaluated EGF ligand by immunohistochemistry (IHC) in H1975 vehicle- and BV-treated xenografts at progression and observed increased levels of EGF immunoreactivity in resistant tumors compared with controls (Supplemental Figure 2B).

We next examined the activation status of EGFR in H1975 and A549 xenografts after treatment with vehicle and BV at progression. Confocal microscopy was used to analyze specimens stained with antibodies directed against CD31 and p-EGFR. As shown in Figure 3B, BV resistance was associated with a marked difference in p-EGFR expression in both H1975 and A549 tumors compared with controls; however, notable differences in the staining pattern were observed between the 2 xenograft models. In the H1975 model, p-EGFR expression was significantly increased on the vascular supporting cells (VSCs) of resistant tumors compared with controls ($P < 0.001$), whereas in A549 BV-resistant xenografts, p-EGFR expression was significantly increased on tumor-associated ECs compared with controls ($P < 0.05$; Figure 3C, right).

To identify the population of VSCs expressing p-EGFR in H1975 BV-resistant tumors, we performed IF staining using antibodies directed against p-EGFR and desmin, a marker for pericytes (Figure 3D). This analysis revealed that the VSCs of H1975 BV-resistant tumors coexpressed p-EGFR and desmin. In addition, the number of pericytes expressing p-EGFR was 8-fold greater in H1975 BV-resistant tumors than in control tumors ($P < 0.01$; Figure 3E). Taken together, our results suggest that upregulation and activation of stromal EGFR is a characteristic feature of BV-resistant tumors in these models and that multiple stromal cell types can express EGFR.

Increased expression of basic FGF and FGFR2 in H1975 xenografts resistant to BV therapy. Based on our observation that mouse *Fgfr2* gene expression was increased in the stromal compartment of BV-resistant H1975 tumors, we performed colocalization studies (IF) on H1975 tumors that progressed while receiving vehicle and BV, using antibodies against CD31 and FGFR2 (Figure 4A). We observed a significant increase in FGFR2 protein expression levels in resistant tumors compared with controls ($P < 0.001$; Figure 4B). Furthermore, to assess changes in the FGFR2 ligand, we next measured the plasma concentration of mouse basic FGF (bFGF). We found a 1.5-fold increase in the level of circulating bFGF in BV-resistant tumors compared with controls ($P = 0.025$; Figure 4C). Consistent with these findings, IHC analysis of H1975 control- and BV-treated xenografts at progression demonstrated increased protein expression of bFGF in BV-resistant tumors compared with controls (Figure 4D).

Resistance to BV is associated with tumor revascularization and morphological changes in the vasculature. Because the primary mechanism of action of BV is directed against blood vessels, we quantified the microvessel density (MVD) of H1975 and A549 xenografts. We initially assessed changes in the vasculature after short-term treatment. There was a 3-fold MVD reduction in initially sensitive H1975 tumors treated with BV for 2 weeks compared with controls ($P < 0.01$; Figure 5, A and B). Vessel density (as an indicator of relative primary resistance) of A549 tumors treated for 2 weeks did not show significant changes compared with controls. To determine whether the vascular effects observed after 2 weeks of BV therapy persisted in tumors receiving long-term BV treatment, we quantified the MVD in BV-resistant H1975 and A549 tumors (Figure 5, A and B). We found that relative primary and acquired resistance were associated with distinct patterns of tumor vascularization. In H1975 BV-treated xenografts, MVD was significantly higher at progression compared with 2 weeks of treatment ($P < 0.01$), then returned to levels comparable to those of vehicle-treated controls. In A549 BV-resistant xenografts, MVD significantly increased compared with A549 vehicle-treated controls ($P < 0.05$). These data suggest that BV therapy has a marked initial antiangiogenic effect on sensitive H1975 xenografts, but the effect is lost after continued exposure to the drug, and that therapeutic resistance is associated with revascularization at levels comparable with or higher than those in vehicle-treated controls.

Previous studies have demonstrated that antiangiogenic therapy can alter the morphology of the tumor-associated vasculature (29–32). To evaluate the tumor vascularization in greater detail, we measured the vascular tortuosity in vehicle and BV-treated H1975 and A549 xenografts. Short-term administration of BV led to a modest, but not statistically significant, reduction in the vessel tortuosity of H1975 tumors (Figure 5, A and C). However, as these tumors developed BV resistance, we noted a 4-fold reduction in vascular tortuosity compared with controls ($P < 0.01$). These blood vessels were also characterized by large-diameter lumens and a greater degree of pericyte coverage (referred to herein as normalized revascularization). In contrast, in A549 xenografts with relative primary resistance to BV, tumor vascularization was associated with smaller, more tortuous vessels with reduced pericyte coverage compared with controls (referred to herein as sprouting vascularization; $P < 0.05$; Figure 5, A and C). Thus, in these mod-

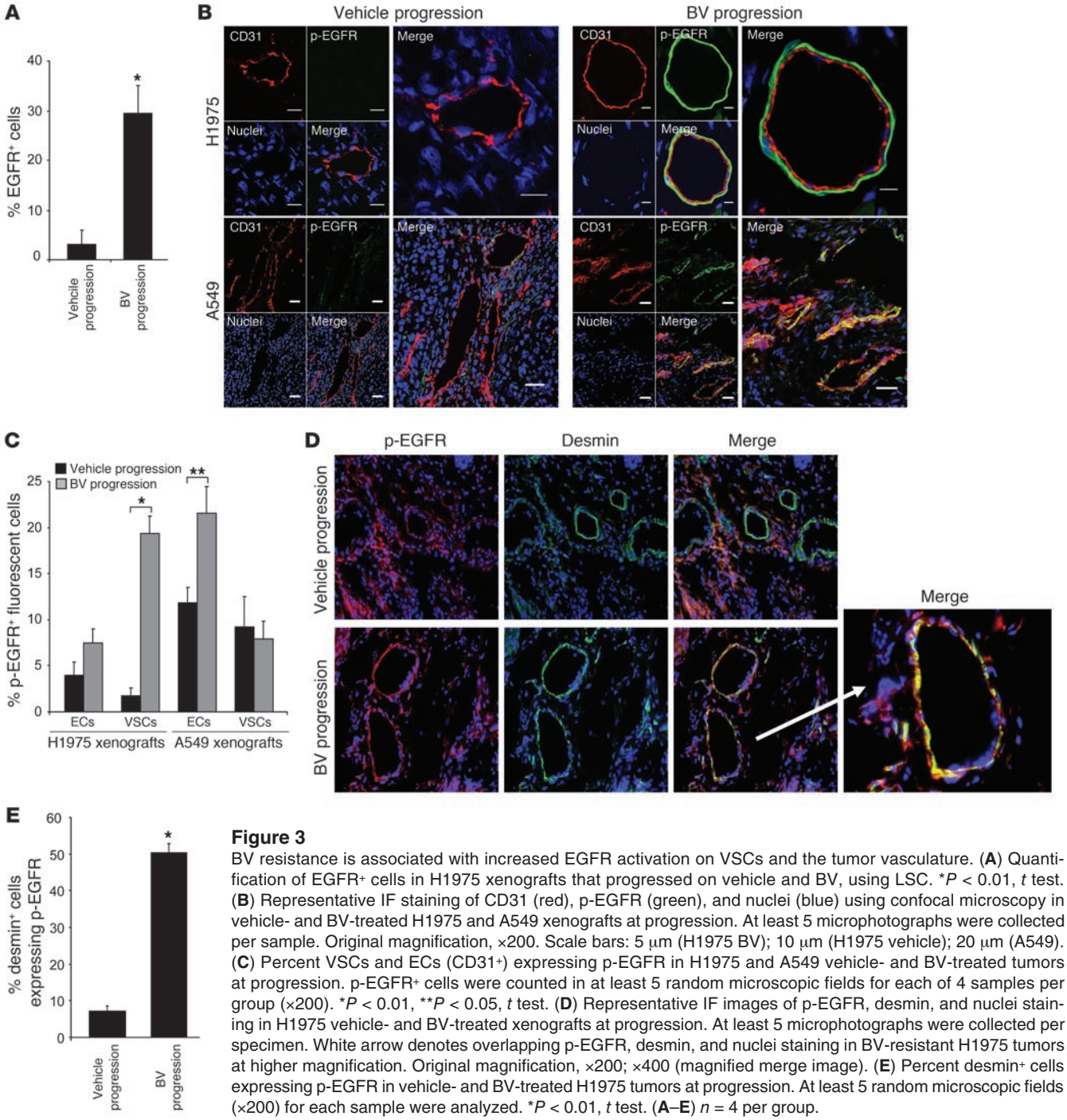

Figure 3

BV resistance is associated with increased EGFR activation on VSCs and the tumor vasculature. (**A**) Quantification of EGFR+ cells in H1975 xenografts that progressed on vehicle and BV, using LSC. *$P < 0.01$, *t* test. (**B**) Representative IF staining of CD31 (red), p-EGFR (green), and nuclei (blue) using confocal microscopy in vehicle- and BV-treated H1975 and A549 xenografts at progression. At least 5 microphotographs were collected per sample. Original magnification, ×200. Scale bars: 5 μm (H1975 BV); 10 μm (H1975 vehicle); 20 μm (A549). (**C**) Percent VSCs and ECs (CD31+) expressing p-EGFR in H1975 and A549 vehicle- and BV-treated tumors at progression. p-EGFR+ cells were counted in at least 5 random microscopic fields for each of 4 samples per group (×200). *$P < 0.01$, **$P < 0.05$, *t* test. (**D**) Representative IF images of p-EGFR, desmin, and nuclei staining in H1975 vehicle- and BV-treated xenografts at progression. At least 5 microphotographs were collected per specimen. White arrow denotes overlapping p-EGFR, desmin, and nuclei staining in BV-resistant H1975 tumors at higher magnification. Original magnification, ×200; ×400 (magnified merge image). (**E**) Percent desmin+ cells expressing p-EGFR in vehicle- and BV-treated H1975 tumors at progression. At least 5 random microscopic fields (×200) for each sample were analyzed. *$P < 0.01$, *t* test. (**A**–**E**) $n = 4$ per group.

els, acquired resistance and relative primary resistance to BV were associated with distinct patterns of vascular remodeling.

Dual blockade of EGFR and VEGFR2 signaling pathways delays tumor growth of NSCLC xenografts. To elucidate whether targeting functioning stromal signaling pathways in BV-resistant tumors abrogates therapeutic resistance, we targeted EGFR using either the EGFR TKI erlotinib in combination with BV, or the dual VEGFR/EGFR inhibitor vandetanib. Both A549 and H1975 tumor cells are known to be resistant to erlotinib and vandetanib in vitro, which is thought to be caused by the presence of a KRas mutation and a secondary EGFR mutation (T790M), respectively (26–28). Consistent with previous results, erlotinib did not inhibit H1975 tumor growth compared with vehicle, as 5 of 6 xenografts progressed, with a median PFS of 12.5 days ($P = 0.33$, erlotinib versus vehicle; Figure 6A). Erlotinib and BV treatment in combination (referred to herein as erlotinib+BV) resulted in prolonged PFS; only 1 of 6 tumors progressed at the end of more than 200 days (median PFS not reached; $P = 0.0009$, erlotinib+BV versus vehicle; $P = 0.19$, erlotinib+BV versus BV; Figure 6, A and B), although after more than 140 days of treatment, 3 mice died of causes unrelated to

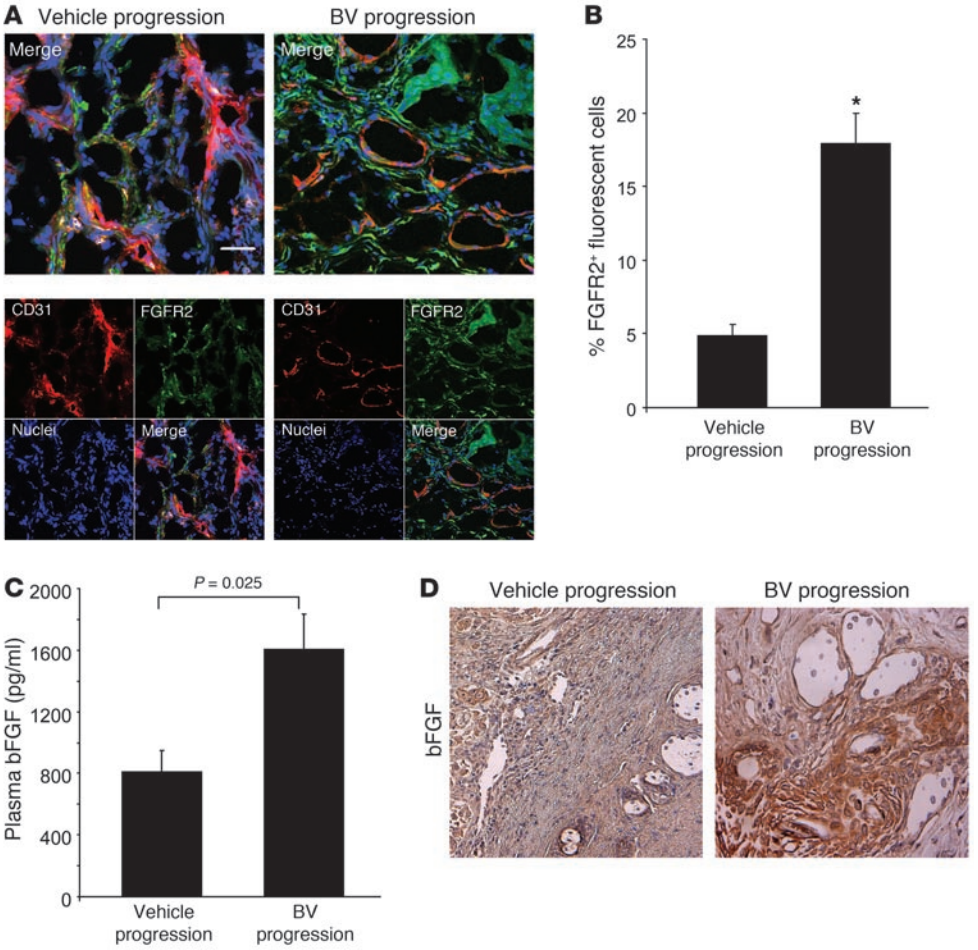

Figure 4
Increase in stromal FGFR2 expression in H1975 BV-resistant xenografts. (**A**) Representative IF images of CD31 and FGFR2 staining in H1975 vehicle- and BV-treated H1975 xenografts at progression, using confocal microscopy. At least 5 microphotographs were collected from 4 specimens per group. Original magnification, ×200. Scale bar: 20 μm. (**B**) Percent FGFR2+ fluorescent cells counted in 5 random microscopic fields (×200) per sample (n = 4 per group). *P < 0.001, t test. (**C**) bFGF levels were measured in plasma of vehicle- and BV-treated H1975 xenografts at progression, using multiplex bead assay (n = 4 per group; each sample tested in duplicate). P value was calculated using t test. (**D**) Representative IHC images showing bFGF protein expression in vehicle- and BV-treated H1975 xenografts. At least 5 random microscopic fields were collected from each of 4 specimens per group. Original magnification, ×200.

tumor growth. Vandetanib treatment inhibited tumor growth in all tumors, and only 2 of 6 progressed after response, displaying a median PFS of 211 days (P = 0.0007, vandetanib versus vehicle; P = 0.295, vandetanib versus BV; Figure 6, A and B).

In A549 xenografts, treatment with erlotinib resulted in a median PFS of 53 days, compared with 29.5 days in vehicle-treated controls (P = 0.34; Figure 6C). Over the course of the experiment, 2 tumors progressed on erlotinib+BV treatment (median PFS not reached), and the addition of erlotinib to BV significantly delayed the onset of resistance compared with BV alone (P = 0.013, erlotinib+BV versus vehicle; P = 0.049, erlotinib+BV versus BV; Figure 6, C and D). On vandetanib treatment, 1 xenograft progressed after 102 days, and the median PFS was not reached (P = 0.017, vandetanib versus vehicle; P = 0.046, vandetanib versus BV; Figure 6, C and D). These findings indicate that EGFR inhibition not only reduced the number of NSCLC xenografts that progressed on therapy compared with BV alone in both our models, but also delayed the onset of resistance to VEGF signaling inhibition in A549 xenografts.

Given the aforementioned EGFR expression in pericytes in the H1975 model, we examined whether targeting EGFR affects vessel maturation and pericyte coverage. Multicolor IF staining was performed using antibodies directed against CD31 and desmin, and pericyte coverage was quantified. In H1975 BV-resistant xenografts, the percentage of blood vessels supported by pericytes was 50% greater than that in control tumors (P < 0.01; Figure 5D). However, pericyte coverage was significantly reduced in tumors receiving long-term treatment with erlotinib+BV or with vandetanib (P < 0.01), consistent with EGFR blockade blunting the increase in pericyte coverage accompanying the normalized revascularization observed with BV in this model. In contrast, A549 xenografts that progressed on BV therapy had significantly fewer blood vessels supported by pericytes than did controls (P < 0.01; Supplemental Figure 3); nevertheless, long-term administration of erlotinib+BV or of vandetanib also decreased the pericyte coverage in this model compared with controls (P < 0.01; Supplemental Figure 3), providing further support for the role of EGFR in tumor-associated stroma.

Lung adenocarcinoma H441 orthotopic tumors acquire resistance to BV, and tumor growth is delayed with dual EGFR/VEGFR2 inhibition. To investigate whether the changes associated with BV resistance in subcutaneous models also occur in tumors growing in the lung, we used an established orthotopic model whereby H441 lung adenocarcinoma cells were injected directly into the lung of male nude mice. These cells harbor wild-type EGFR and mutant KRas and were selected because of their moderate tumor cell resistance to EGFR blockade (33), and also because they display optimal growth kinetics when implanted in the mouse lung (34). At 21 days after injection, an initial cohort of 8 mice was euthanized to evaluate mean tumor volume (approximately 60 mm^3). To evaluate the effects of short-term BV treatment, 2 additional groups of mice were sacrificed after 2 weeks of BV therapy, as in the prior experiments. The remaining animals were then randomized for a

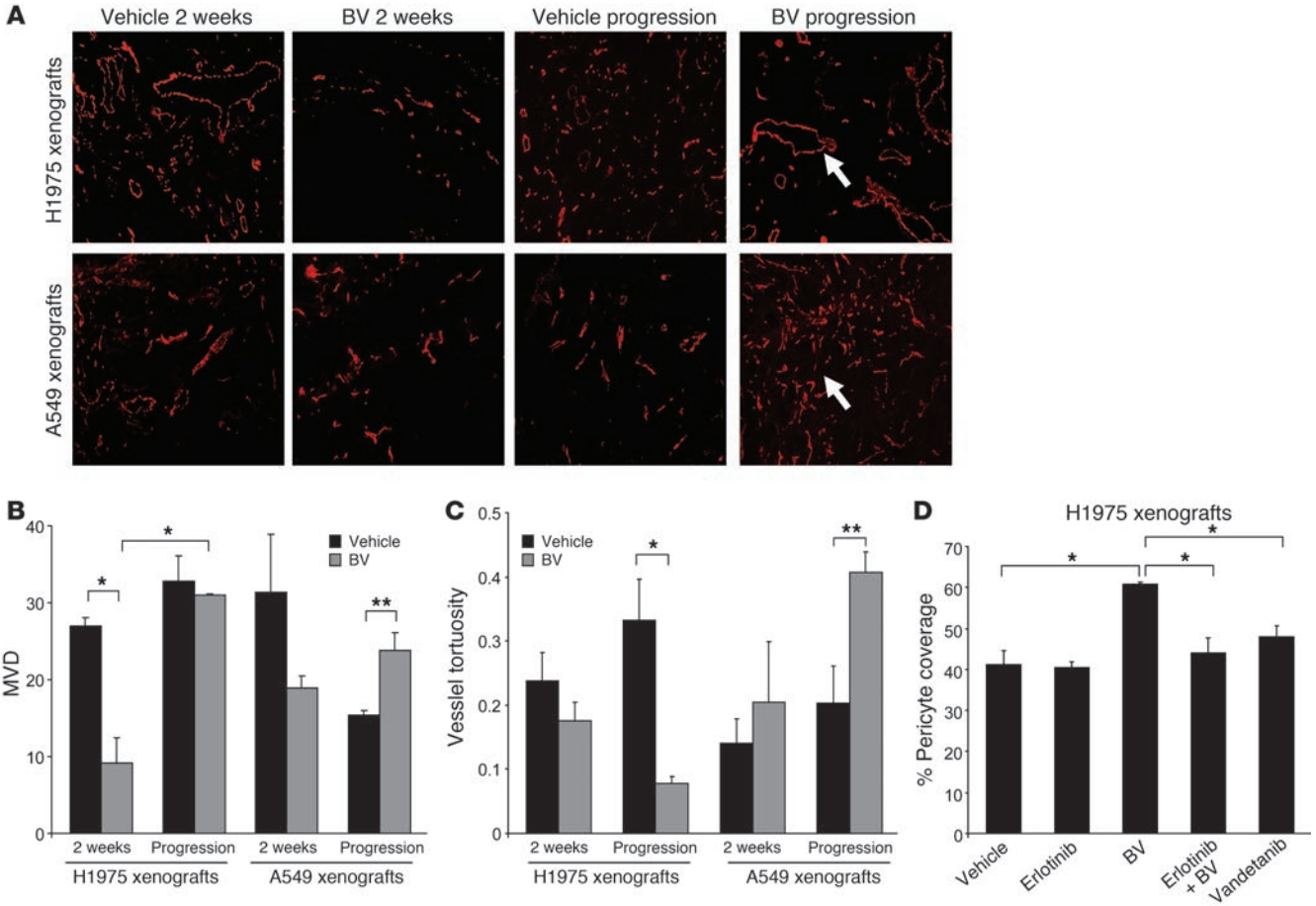

Figure 5

Altered patterns of tumor vascular density, tortuosity, and pericyte coverage in BV-resistant xenograft tumors. (**A**) Microphotographs of CD31$^+$ tumor vessels (red) in H1975 and A549 xenografts treated with vehicle and BV after 2 weeks and at progression. 5–10 microscopic fields were collected from each of 4 specimens per group. Arrows indicate the different vessel morphology in H1975 (top panel) and A549 (lower panel) BV-resistant tumors. Original magnification, ×100. (**B** and **C**) Quantification of MVD (**B**) and vessel tortuosity (**C**) based on CD31-stained tumor sections in H1975 and A549 xenografts treated with vehicle and BV after 2 weeks and at progression. 5 hotspot microscopic fields (×200) per tumor section were analyzed to quantify MVD; 5 random microscopic fields (×100) were quantified for vessel tortuosity analysis. $n = 4$ per group. Units of the y axis for MVD (**B**) represent CD31 + vessels per HPF (high power field). The y axis for vessel tortuosity (**C**) represents the ratio T = (L/S) – 1. (**D**) Pericyte coverage of H1975 xenografts was quantified as percent CD31$^+$ vessels with at least 50% coverage of associated desmin$^+$ cells in at least 5 microscopic fields (×200) in tumors receiving long-term treatment. $n = 2$ (vandetanib); 3 (erlotinib); 4 (vehicle, BV, and erlotinib+BV). (**B**–**D**) $^*P < 0.01$, $^{**}P < 0.05$, t test.

survival analysis ($n \geq 7$ per group) and treated with vehicle, erlotinib, BV, erlotinib+BV, or vandetanib until moribund, at which time they were euthanized. Survival was defined as the time from treatment onset until sacrifice.

Short-term treatment with BV resulted in significant tumor growth inhibition compared with vehicle-treated tumors ($\Delta T/\Delta C$ 45.7%; $P = 0.026$, Mann-Whitney test; Figure 7, A and B). In the long-term treatment analysis, all mice had a large tumor burden at the time of sacrifice (Figure 7C). As shown in Figure 7D and Supplemental Figure 4, erlotinib treatment resulted in a small but significant prolongation of survival compared with vehicle (median survival, 58 versus 50 days; $P = 0.02$, log-rank test). The BV group had a longer survival (median, 77 days) compared with erlotinib alone ($P = 0.00015$), and the combination of erlotinib and BV, or vandetanib, significantly prolonged survival (median, 101 days) compared with BV or erlotinib alone ($P = 0.0001$, erlotinib+BV versus erlotinib; $P = 0.0001$, erlotinib+BV versus BV; $P = 0.022$, vandetanib versus BV; Figure 7D and Supplemental Figure 4, C and D). Similar to our results obtained with the H1975 xenografts, H441 orthotopic tumors were initially sensitive to VEGF signaling pathway blockade, but tumors ultimately progressed. In this orthotopic model, dual targeting of EGFR and VEGF pathways significantly delayed the onset of therapeutic resistance compared with inhibition of either pathway alone.

Characterization of H441 orthotopic tumor stroma after anti-VEGF therapy and dual EGFR/VEGFR2 inhibition. We next sought to more completely characterize the vasculature and stroma of BV-resistant H441 tumors. We found a significant decrease in MVD after 2 weeks of BV treatment compared with vehicle controls ($P = 0.0008$; Figure 7E). Consistent with the revascularization observed in the subcutaneous models, tumors resistant to BV or dual VEGFR/EGFR inhibition showed significantly increased MVD compared with BV-sensitive

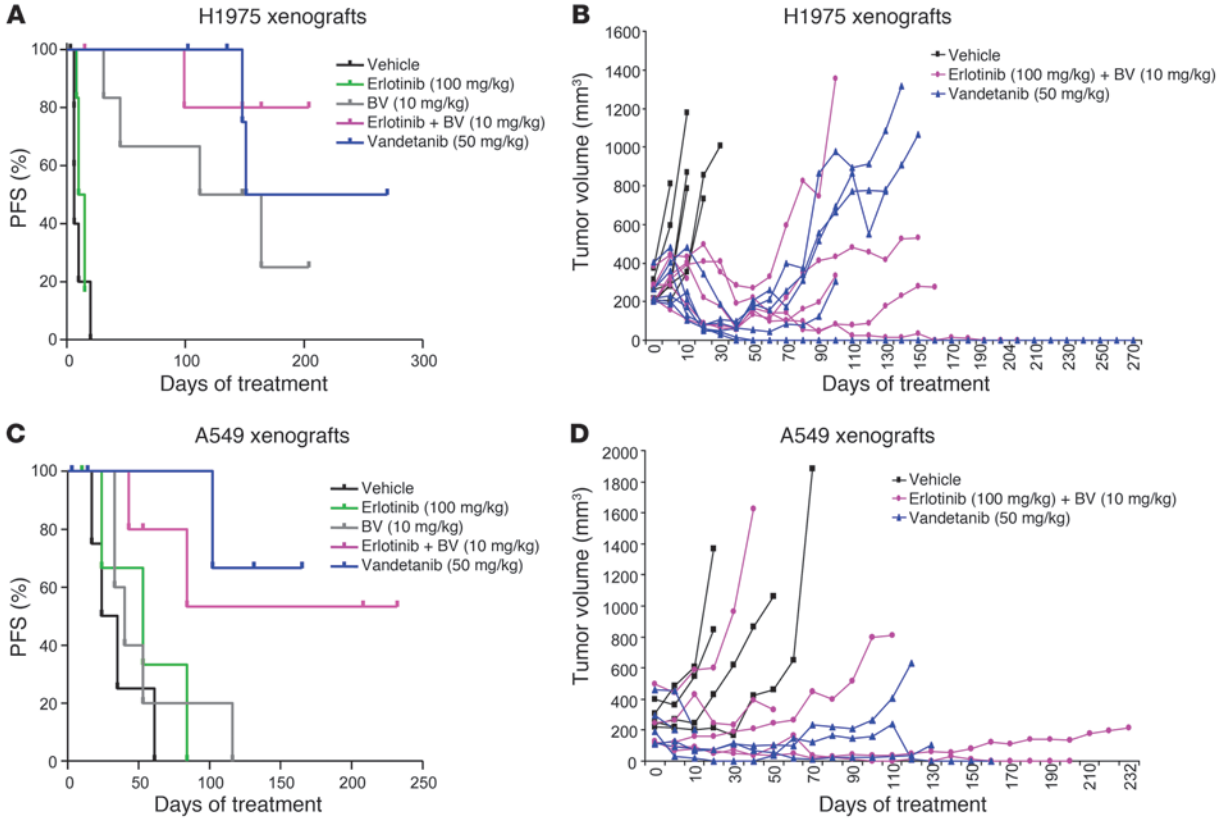

Figure 6
Effect of dual EGFR/VEGFR2 inhibition on H1975 and A549 NSCLC xenograft models. (**A** and **C**) Distribution of PFS, shown by Kaplan-Meier plots, and (**B** and **D**) individual tumor growth curves of H1975 (**A** and **B**) and A549 (**C** and **D**) xenografts receiving long-term treatment as indicated. Log-rank test was used to compare statistical differences in survival among treatment groups.

tumors ($P = 0.045$; Figure 7E). Interestingly, in the erlotinib-resistant group, no revascularization was observed; in fact, MVD was significantly lower than in BV-resistant tumors ($P = 0.034$; Figure 7E). These findings indicate that VEGF inhibitor resistance is associated with revascularization in H441 orthotopic tumors.

We next investigated the EGFR signaling pathway in BV-resistant H441 tumors. Protein levels of total EGFR were not significantly different in tumor and endothelium of vehicle and BV-resistant H441 tumors (data not shown). Levels of p-EGFR, however, were significantly increased in H441 BV-resistant tumors compared with vehicle-treated tumors ($P = 0.039$; Figure 8, A and B), and, consistent with the H1975 subcutaneous model of acquired resistance, the activated receptor colocalized with the stroma, supporting large, normalized vessels in BV-resistant tumors. Furthermore, in tumors resistant to VEGFR/EGFR targeting, the levels of p-EGFR were strongly decreased compared with either vehicle-treated or BV-resistant tumors ($P = 0.0001$, erlotinib+BV versus vehicle; $P = 0.0008$, erlotinib+BV versus BV; $P = 0.011$, vandetanib versus vehicle; $P = 0.009$, vandetanib versus BV; Figure 8, A and B), demonstrating persistent EGFR blockade with treatment. Given these results, we next quantified the percentage of pericyte coverage of the blood vessels supplying H441 orthotopic tumors, as an index of vessel maturations. As shown in Figure 8, C and D, BV-resistant tumors had significantly increased pericyte coverage compared with controls and BV-sensitive tumors ($P = 0.003$, BV progression versus vehicle progression; $P < 0.0001$, BV progression versus BV 2 weeks). Moreover, in tumors that progressed while receiving erlotinib alone, erlotinib+BV, or the dual inhibitor vandetanib, the pericyte coverage was reduced to levels comparable to vehicle-treated tumors ($P = 0.001$, erlotinib versus BV; $P = 0.054$, erlotinib+BV versus BV; $P = 0.007$, vandetanib versus BV; Figure 8, C and D). These findings support our earlier observation that stromal EGFR contributed to acquisition of resistance to VEGF inhibition through signaling activation on VSCs. However, we also noted in BV-resistant H441 tumors a substantial amount of p-EGFR IF staining localized far from the $CD31^+$ vascular structures (Figure 8A), which indicates that apart from VSCs, other components of the tumor stroma may undergo significant changes and contribute to the resistant phenotype, at least in this model. Furthermore, it is worth noting that increases in FGFR2 gene and protein levels were not observed in BV-resistant orthotopic tumors (data not shown), which indicates that there were differences between the orthotopic and subcutaneous models.

Inflammatory cells and tumor-associated fibroblasts in BV-resistant tumors. Because bone marrow–derived inflammatory cells and tumor-associated fibroblasts have previously been shown to play a role in mediating angiogenesis and refractoriness to VEGF blockade (23, 25, 35, 36), we next evaluated the infiltration of inflammatory macrophages and myofibroblasts in the stroma of both our models of acquired resistance. We performed double IF staining

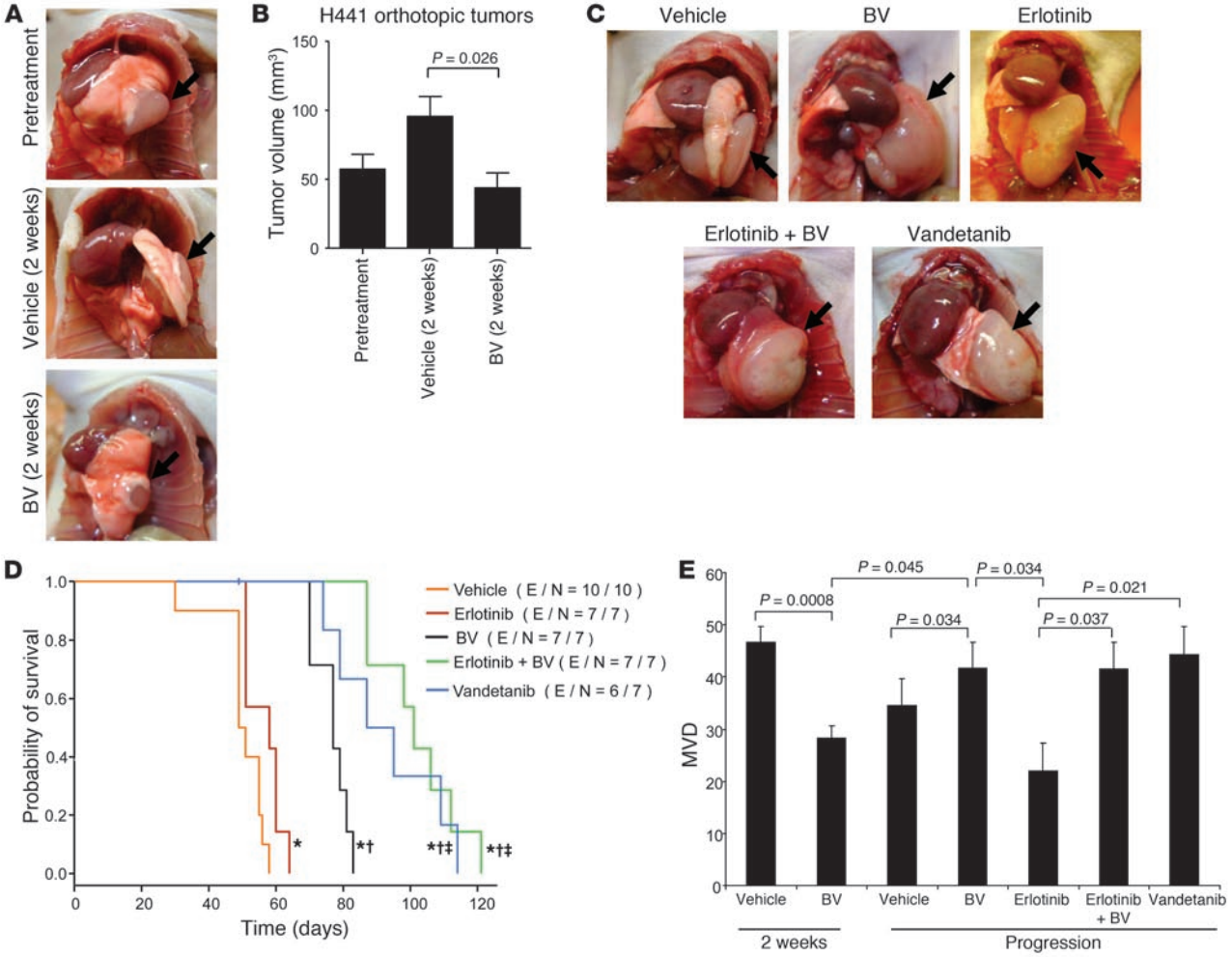

Figure 7

Orthotopic H441 NSCLC tumor growth and MVD after VEGF blockade or dual EGFR/VEGFR pathway inhibition. (**A** and **B**) Representative photographs (**A**) and mean tumor volume obtained at the last measurement (**B**) of H441 orthotopic tumors before or after 2 weeks of treatment. Arrows denote tumor mass in the lung. $n = 8$ (pretreatment); 9 (vehicle); 10 (BV). P value was calculated using Mann-Whitney test. (**C**) Representative photographs of H441 orthotopic tumors after long-term administration. $n = 10$ (vehicle); 7 (erlotinib, BV, and erlotinib+BV); 6 (vandetanib). Arrows denote tumor mass in the lung. (**D**) Kaplan-Meier plots showing survival distribution in H441 orthotopic tumor–bearing mice treated as indicated. Number of events (E) per number in each group (N) is indicated. $^*P < 0.05$ versus vehicle, $^\dagger P < 0.01$ versus erlotinib, $^\ddagger P < 0.05$ versus BV, log-rank test. (**E**) MVD quantification in H441 orthotopic tumors. $n = 4$ (erlotinib); 5 (vehicle 2 weeks and vandetanib); 6 (BV 2 weeks and vehicle progression); 7 (BV progression and erlotinib+BV). Statistical values were calculated using t test. Units in the y axis for MVD represent CD31 + vessels per HPF.

to identify F4/80$^+$ macrophages (Supplemental Figure 5A) and α-SMA$^+$ fibroblasts and myofibroblasts (Supplemental Figure 5C) in both H1975 subcutaneous and H441 orthotopic tumors with BV resistance. As shown in Supplemental Figure 5, B and D, there were no significant differences in overall levels of these markers between vehicle- and BV-treated tumors at progression in either model. In vehicle-treated H441 tumors, the α-SMA staining pattern suggested a dense and desmoplastic stroma. Conversely, this pattern was no longer observed in BV-resistant tumors: α-SMA consistently localized in rounded, well-demarcated areas, indicating a pattern characteristic of, but not limited to, perivascular cells in this model. In fact, given the different localization pattern of α-SMA between BV-resistant orthotopic tumors and vehicle-treated tumors, we cannot rule out the possibility of potential changes in other cell populations of the lung microenvironment, such as mesenchymal or other stromal cells, that might contribute to the onset of resistance to VEGF inhibition.

Discussion

Early reports examining the effects of VEGF blockade and other antiangiogenic therapies raised the hopes that these agents may substantially slow or stop tumor growth, and that therapeutic resistance to these agents would be less likely to occur, at least in part, because the target was diploid and not prone to the same genetic instability as tumor cells (37, 38). However, both preclinical studies and clinical experience in lung cancer and other solid tumors (12, 17, 39–43) indicate that the vast majority of solid tumors either exhibit primary (intrinsic) resistance or will eventually acquire resistance to the effects of antiangiogenic therapy. Although to date most studies of therapeutic resistance to anticancer drugs have

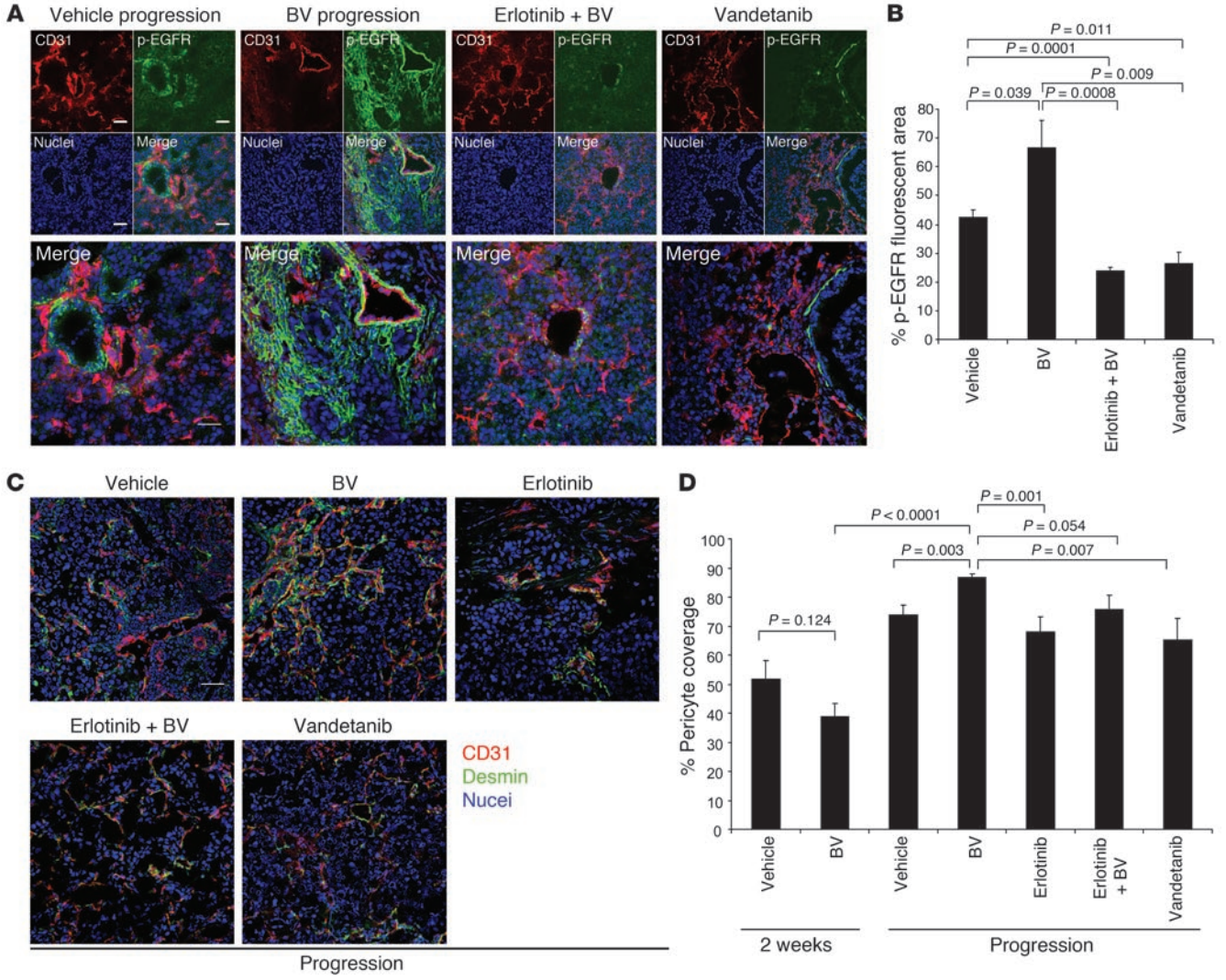

Figure 8

EGFR is activated in H441 BV-resistant tumors, and dual EGFR/VEGFR inhibition reduces pericyte coverage. (**A**) Representative microphotographs of CD31 (red), p-EGFR (green), and nuclei (blue) fluorescent staining in H441 tumors that progressed on vehicle, BV, erlotinib+BV, and vandetanib treatments, using confocal microscopy. At least 5 microphotographs were collected from all the tumor specimens in each group. Original magnification, ×200. Scale bar: 50 μm. (**B**) Percent p-EGFR fluorescent area in H441 tumors that progressed while on the indicated therapies, as determined using Alpha Innotech Software. 5–10 random microphotographs (×200) of red (CD31), green (p-EGFR), and blue (nuclei) fluorescence were collected from 5 (vehicle and BV), 6 (erlotinib+BV), and 4 (vandetanib) specimens per group. *P* values were calculated using *t* test. (**C**) Representative IF images of CD31, desmin, and nuclei in H441 tumors that progressed while on the indicated treatments, using confocal microscopy. At least 5 microphotographs were collected from all the tumor specimens per group. Original magnification, ×200. Scale bar: 50 μm. (**D**) Percent pericyte coverage in H441 tumors was quantified in at least 5 microscopic fields (×200) of tumor specimens. *n* = 4 (erlotinib); 5 (vehicle 2 weeks and vandetanib); 6 (BV 2 weeks and vehicle progression); 7 (BV progression and erlotinib+BV). *P* values were calculated using *t* test.

focused on the role of tumor cells, recent studies have suggested that host factors, including tumor stroma, may play an important role in resistance to angiogenesis inhibitors (14, 15, 23, 25, 42, 44).

In this study, we used mouse- and human-specific profiling of human NSCLC xenografts in mice to investigate stromal and tumor cell changes occurring in tumors that acquired resistance to BV. This analysis revealed that changes in gene expression, and particularly changes in angiogenesis-related genes, occurred predominantly in stromal and not tumor cells. This observation reinforces the notion that tumor stroma may play an important — and potentially dominant, in at least some circumstances — role in VEGF inhibitor resistance.

Pathway analyses highlighted that among these stromal changes, there were multiple genes in the *Egfr* and *Fgfr2* pathways that were upregulated in resistant tumors (e.g., *Epgn*, *Areg*, *Fgf13*, and *Fgfbp1*) and that the EGFR pathway appeared to be a central gene interaction pathway. EGFR and FGFR2 upregulation was confirmed using species-specific RT-PCR as well as IHC. As noted below, upregulation of the bFGF/FGFR2 pathway has previously been observed by our group and others in VEGF inhibitor resistance

(16, 17, 45), but to our knowledge, a role for stromal EGFR has not been reported previously. We therefore investigated this pathway in greater detail using 3 models: subcutaneous and orthotopic models of acquired resistance (H1975 and H441, respectively) and a model of relative primary resistance (A549). Tumor cells from all 3 models are known to be relatively resistant to EGFR blockade in vitro (26, 33).

In both models of acquired BV resistance, there was a significant increase in activated EGFR that largely, but not exclusively, localized on VSCs, which were predominantly pericytes (Figures 3, 5, and 8). No significant p-EGFR was detectable on VSCs of control tumors. This was accompanied by an increase in pericyte coverage and a pattern of less tortuous, normalized revascularization in the BV-resistant tumors. Dual inhibition of VEGFR and EGFR pathways reduced pericyte coverage of tumor vessels compared with BV alone, which indicates that EGFR signaling plays a functional role in pericyte coverage of tumor vessels in the models studied. Dual targeting also significantly delayed the emergence of resistance and prolonged survival in the H441 model, with similar trends observed in the H1975 model (Figures 6 and 7). To our knowledge, this is the first evidence demonstrating a potential role for EGFR signaling in pericytes or other stromal cell populations of the tumor microenvironment in resistance to VEGF pathway inhibition in murine models of NSCLC.

Consistent with our observation regarding EGFR in tumor pericytes, a recent study found that the EGFR TKI gefitinib significantly suppressed tumor-associated pericyte function (46). During the revisions of this manuscript, other investigators reported a role for the stromal heparin-binding Egf/Egfr (Hb-Egf/Egfr) signaling pathway in the progression of a pancreatic neuroendocrine tumor model of EGFR-targeted inhibition (47). The authors demonstrate that stromal cell–derived Hb-Egf activates the EGFR pathway in perivascular cells, contributing to increased pericyte coverage and angiogenesis. These reports provide further support for a role of EGFR signaling in pericyte function in tumor revascularization.

A recent study has identified a role for PDGF-C expressed by tumor-associated fibroblasts in VEGF inhibitor resistance (25) and in attenuating tumor response to anti-VEGF treatment in a model of glioblastoma (48). PDGFR signaling in pericytes has also been implicated in vessel maturation, and recent evidence indicates that VEGF signaling suppresses pericyte PDGFR signaling, inhibiting vessel maturation (49). Somewhat surprisingly, we did not observe upregulation of any PDGFRs or ligands. In contrast, we noted modest but statistically significant downregulation of the stromal genes *Pdgfa*, *Pdgfb*, and *Pdgfrb*. Given the role of the PDGF family in multiple tumor processes, including pericyte recruitment and function (50, 51), it appears that pericyte-expressed EGFR may play a complimentary or compensatory role in the increased pericyte coverage observed in the acquired resistance models. Although the current study does not address this issue, it will be interesting to determine whether increased pericyte EGFR signaling in the H441 model (in the absence of increased EGFR gene or protein levels) is driven by increased ligand production or by reduced VEGFR-driven inhibition of signaling, as observed for pericyte PDGFR.

In the A549 model, stromal EGFR was also upregulated in BV-resistant tumors, but was localized exclusively to tumor endothelium, not VSCs. As expected, dual VEGFR/EGFR inhibition did not reduce pericyte coverage in this model, but did significantly delay the emergence of resistance compared with BV alone (Figure 6). This observation highlights that a signaling pathway may play different roles in tumor stroma depending on the cellular context. Studies examining EGFR distribution on endothelium suggest that it is restricted to blood vessels supplying pathologic tissues (52), where it activates angiogenic programs (53). Others have reported that EGFR is activated on endothelium when tumor cells express EGFR ligands, such as TGF-α or EGF (54, 55).

Activation of the bFGF/FGFR2 pathway has previously been shown to be a critical regulator of the angiogenic switch (56) and to be upregulated in response to antiangiogenic therapy (17). We observed an approximately 6-fold increase in stromal *Fgfr2* gene expression in tumors with acquired resistance and, consistent with this finding, an increase in the number of FGFR2-expressing cells in these tumors. This immunoreactivity appeared to be largely, but not exclusively, on tumor endothelium. This suggests that the FGFR2 pathway may promote VEGF-independent endothelial survival, as previously observed in other preclinical models (57, 58), although we cannot rule out the possibility that it plays a role in other nonendothelial stromal cells. Circulating levels of bFGF were also elevated in the plasma of mice bearing BV-resistant tumors. This observation is notable in light of our recent observation that acquired resistance to chemotherapy and BV in colorectal cancer patients is associated with an increase in circulating bFGF (45), which suggests that similar mechanisms may be occurring in cancer patients.

The mechanisms underlying regulation of tumor stromal genes altered in resistant tumors remain to be established and are likely to differ in the various stromal cell types. Expression of many of the genes, including *CAIX*, *FGFR2* (59), and *EGFR* family members, is known to be regulated by hypoxia or to correlate with expression of HIF1α, as previously reviewed (60). One possible explanation is that BV therapy initially triggers a substantial decrease in tumor MVD and increases tumor hypoxia (61), inducing upregulation of hypoxia-dependent pathways. It is worth noting, however, that BV resistance was not associated with significant increases in many stromal genes known to be upregulated by hypoxia, and many of the genes upregulated in BV resistance are not known to be regulated by hypoxia. Hypoxia is therefore likely to be only one of many factors — both host and tumor cell dependent — likely to affect the resistant tumor and its microenvironment. These regulators of the stromal response merit further investigation.

Resistance to VEGF inhibition was also associated with different patterns of vascular remodeling in the models of acquired and primary resistance. In the H1975 model of acquired resistance, short-term treatment with BV during the sensitive phase initially induced a reduction in MVD; an increase in EC apoptosis, as observed in other studies (29, 30, 32, 62–65); and tumor shrinkage. This was followed by the development of resistance, marked by a pattern of normalized revascularization with increased MVD, reduced EC apoptosis, and a higher degree of pericyte coverage (Figure 5 and Supplemental Figure 1). These effects appeared to be VEGFR2 independent, as VEGFR2 phosphorylation remained inhibited in resistant tumors. Similar normalized revascularization was observed in the H441 orthotopic model (Figures 7 and 8). Prior studies have indicated that pericyte coverage may exert a protective effect on tumor endothelium (66, 67), potentially through the production of factors promoting endothelial survival and VEGF independence. Our findings were consistent with this hypothesis and revealed pericyte EGFR signaling to be a potential mediator of this effect.

In the A549 model of relative primary resistance, a distinct pattern of disorganized sprouting revascularization was observed in resistant tumors. This was marked by decreases in pericyte cover-

age with BV treatment and increased vessel tortuosity in resistant tumors. Unlike the acquired resistance models, stromal p-EGFR was upregulated in tumor endothelium, which suggests that the endothelium may be able to switch its dependence from VEGFR- to EGFR-driven endothelial proliferation and angiogenesis in the BV-resistant A549 xenografts, resulting in sprouting revascularization. It is worth noting that in an earlier study, we observed a similar switch (from EGFR- to VEGFR-dependent tumor endothelium) in a melanoma model (68), supporting the feasibility of this proposed mechanism. Endothelial EGFR signaling may explain, at least in part, the intrinsic relative resistance of these tumors to VEGF blockade, as well as our prior observation that A549 cells display EGFR TKI resistance in vitro, but show moderate sensitivity to EGFR inhibition when grown as xenografts (26). Other pathways that may contribute to this vascular phenotype are currently under investigation, including regulators of EC motility (e.g., HGF/c-MET) and vessel maturation (e.g., Ang-2/Tie-2). Nevertheless, this model provides evidence that there are distinct patterns of vascular remodeling that can accompany VEGF inhibitor resistance–associated tumor revascularization.

This study has a number of clinical implications for the use of VEGF inhibitors in NSCLC and other tumor types. First, it suggests that dual inhibition of the VEGFR and EGFR pathways may delay the emergence of therapeutic resistance in NSCLC. Consistent with this possibility, a recent phase III study (ATLAS) comparing the use of BV combined with erlotinib versus BV alone as maintenance therapy after chemotherapy demonstrated a significant, but modest, PFS improvement with an observed hazard ratio of 0.72 (P = 0.001; refs. 69, 70). Combined VEGFR/EGFR inhibition (via BV with erlotinib or vandetanib) has also demonstrated significantly improved PFS compared with EGFR inhibition alone (71–73). These studies showed a significant delay in tumor progression while treatment with VEGFR/EGFR inhibition was ongoing; however, significant improvements in overall survival were not observed. The explanation for this lack of durable clinical benefit is not known, but it is possible that once the dual inhibition is discontinued, these 2 pathways, or other alternative escape pathways, rapidly emerge.

The results of the present study may not be broadly generalizable to other tumor types or regimens containing chemotherapy. In a randomized phase III trial in colorectal cancer, the addition of the EGFR monoclonal antibodies panitumumab (74) or cetuxumab (75) to BV and chemotherapy showed trends toward worse clinical outcomes. Furthermore, in a recent study of colorectal cancer patients treated with BV plus chemotherapy, we observed increases in plasma bFGF, HGF, PDGF, and several myeloid factors prior to development of progressive disease (45); in contrast, in our model, bFGF was the sole factor that significantly increased. This suggests that resistance mechanisms may be disease or regimen specific.

Second, these findings raise the possibility that combinations of VEGF inhibitors with drugs targeting other potential stromal resistance pathways — such as FGFR2 — may improve treatment efficacy. Third, they suggest that the analysis of both tumor cell and stromal markers — not just tumor cell markers alone — may provide important clinical information. Fourth, they suggest that analysis of vascular patterns in VEGF inhibitor–resistant tumors may provide information regarding the underlying mechanisms of resistance.

In summary, our findings suggest that in NSCLC models, gene expression changes associated with VEGF inhibitor resistance occur predominantly in tumor stromal cells, not tumor cells, providing further evidence that tumor stroma may play an important — and potentially dominant — role in VEGF inhibitor resistance. Primary and acquired resistance may be associated with distinct patterns of vascularization, described here as normalized and sprouting patterns, and distinct patterns of stromal signaling. Finally, we identify what we believe to be a novel role for pericyte EGFR signaling in VEGF inhibitor resistance. It is worth noting, however, that although combinations of VEGF and EGFR pathway inhibition have shown promise in NSCLC, therapeutic resistance nevertheless continues to emerge, which indicates that additional resistance mechanisms remain to be uncovered.

Methods

Subcutaneous in vivo studies. All animal studies reported were approved by M.D. Anderson Cancer Center's animal care committee, which is fully accredited by the Association for Assessment and Accreditation of Laboratory Animal Care (AAALAC International). To generate tumor xenografts, A549 and H1975 tumor cells (2.0×10^6) in 100 μl HBSS were injected into the subcutaneous flanks of 4- to 8-week-old male athymic nude mice (NCI-nu). Body weights and tumor volumes were recorded twice weekly. Tumor volumes were calculated as $\pi/6 \times a^2 \times b$, where a is the smaller measurement of the tumor and b is the larger one, and expressed in cubic millimeters. When the tumor volumes reached an average of approximately 270 mm^3, mice were randomly assigned to one of the following treatment groups: (a) control i.p. injection of vehicle (PBS) twice weekly and oral (p.o.) administration of vehicle daily; (b) i.p. injection of BV (10 mg/kg) twice weekly; (c) erlotinib (100 mg/kg) p.o. daily; (d) erlotinib p.o. daily plus BV i.p. twice weekly; (e) vandetanib (50 mg/kg) p.o. daily (n = 6 [H1975] and 5 [A549] per group). Animals were sacrificed due to tumor burden. The log-rank test was performed to compare survival curves between different treatment groups using GraphPad Prism version 5.00 for Windows (GraphPad Software). For short-term treatment studies, H1975 (n = 5 per group) and A549 (n = 6 per group) tumor-bearing animals were treated for 2 weeks with vehicle and BV (10 mg/kg) and then sacrificed. The last tumor measurement was used to calculate $\Delta T/\Delta C$ (change in tumor volume relative to change in control, expressed as a percentage), as previously described (76). Tumor tissues from short- and long-term in vivo experiments were collected for IHC studies. Tumors were excised, a portion was fixed in formalin and embedded in paraffin, and another portion was embedded in OCT (Miles Inc.) and rapidly frozen in liquid nitrogen. Additional tumor sections for molecular studies were snap-frozen in liquid nitrogen. Staining with H&E was used to confirm the presence of tumor in each sample included in the analysis.

RNA microarray analysis. Total RNA was extracted from snap-frozen tissues using the *mir*Vana miRNA Isolation Kit (Ambion) according to the manufacturer's protocol. Biotin-labeled cRNA samples for hybridization were prepared using Illumina Total Prep RNA Amplification Kit (Ambion Inc.). Total RNA (1 μg) was used for the synthesis of cDNA, followed by amplification and biotin labeling. Each of 1.5 μg of biotinylated cRNAs was hybridized to both mouse WG-6v2 and human WG-6v3 Expression BeadChips (Illumina) at the same time for analysis of murine and human transcriptomes. Signals were developed by Amersham fluorolink streptavidin-Cy3 (GE Healthcare). Gene expression data were collected using an Illumina bead Array Reader confocal scanner (BeadStation 500GXDW; Illumina Inc.). Data were analyzed using the BRB-ArrayTools Version 3.7.0 Beta platform (http://linus.nci.nih.gov./BRB-ArrayTools.html). A log base-2 transformation was applied to the data set prior to data normalization. A median array was selected as the reference array for normalization, and statistical significance was set at $P < 0.01$. To evaluate the expression of genes involved in response to hypoxia, lymphangiogenesis, and angiogenesis in

BV-resistant xenografts versus controls, a list of 269 genes used in previous publications was compared (77). Genes differentially expressed between groups were determined applying univariate *t* test with estimation of the false discovery rate (FDR). Genes were determined using selection criteria of $P < 0.005$ and fold change of 1.5 or larger. Functional gene-interaction network analysis of genes differentially expressed between the mouse stroma of BV-resistant and vehicle-treated H1975 xenografts was performed using Ingenuity Pathways Analysis.

Accession numbers. Microarray data have been deposited into NCBI GEO (accession no. GSE26644).

IF. Frozen tissue sections were used to evaluate CD31, p-VEGFR2, EGFR, and desmin expression. Specimens were sectioned (8–10 μM thickness), mounted onto positively charged slides, and air-dried for 30 minutes. Tissue fixation was performed using 3 sequential immersions in ice-cold acetone, acetone-chloroform 50:50 (v/v), and acetone (5 minutes each). Slides were incubated in protein block solution containing 4% fish gelatin for 20 minutes at room temperature and then incubated overnight at 4°C with a 1:500 dilution of rat anti-mouse CD31. Sections were rinsed with PBS and then incubated for 1 hour with a goat anti-rat Alexa Fluor 594 antibody (diluted 1:1,200). Samples were rinsed with PBS, incubated for 20 minutes with protein block, and then incubated with primary antibody against p-VEGFR2 (diluted 1:400), or EGFR (diluted 1:100) or desmin (diluted 1:400) at 4°C overnight. Samples were rinsed 3 times with PBS and then incubated for 1 hour with goat anti-rabbit Alexa Fluor 488 antibody (diluted 1:1,200). After rinsing, sections were incubated with Hoechst stain (diluted 1:10,000 in PBS; Polysciences Inc.) for 2 minutes to visualize cell nuclei. Slides were mounted with a glycerol/PBS solution containing 0.1 mol/l propyl gallate (Sigma-Aldrich) to minimize fluorescent bleaching. IF microscopy was performed using a Zeiss Axioplan fluorescence microscope (Carl Zeiss Inc.) equipped with a 100-W Hg lamp and narrow bandpass excitation filters. Representative images were obtained using a cooled charge-coupled device Hamamatsu C5810 camera (Hamamatsu Photonics) and Optimas software (Media Cybernetics).

Confocal microscopy. Confocal microscopy was used in protein localization studies of CD31 and p-EGFR and of CD31 and total FGFR2 in subcutaneous murine models, and of CD31 and desmin, CD31 and p-EGFR, and F4/80 and α-SMA staining in orthotopic tumors, as previously described (78). Frozen tissues for confocal microscopy were sectioned (8–12 μm) and mounted on positively charged slides. IF staining for p-EGFR or total FGFR2 and CD31 was carried out as described above, with the exception that the Alexa Fluor 594 fluorophore used for CD31 detection was replaced with a Cy5 antibody, and the Alexa Fluor 488 fluorophore used to visualize p-EGFR or FGFR2 or desmin was replaced with a Cy3 antibody. Sytox green (diluted 1:10,000 in PBS) was used to visualize cell nuclei. Confocal fluorescence images were collected using a Zeiss LSM 510 laser scanning microscope (Carl Zeiss Inc.) equipped with an argon laser (458/477/488/514 nm, 30 mW), HeNe laser (413 nm, 1 mW and 633 nm, 5 mW), LSM 510 control and image acquisition software, and appropriate filters (Chroma Technology Corp.).

Determination of MVD, vessel tortuosity, and pericyte coverage. Tumor MVD was determined as previously described (79). In brief, we examined tumors microscopically to identify hot spots by low magnification (×100), and the mean MVD was quantified as the total number of $CD31^+$ structures observed in at least 5 higher-magnification microscopic fields per tumor (×200). For each group, tumors from 4 mice receiving short- and long-term treatment were used. As previously described (80), the tortuosity of blood vessel was calculated as $(L/S) - 1$, where L is the length of the vessel of interest and S is the straight-line distance between its endpoints. Vessel length was evaluated in 4 samples per treatment group by tracing along the midline of the blood vessels that showed up in a longitudinal cut within an image (×100), and the number of pixels was converted into distance in millimeters with NIH ImageJ (version 1.34; http://rsb.info.nih.gov/ij/). To determine the extent of pericyte coverage on the tumor vasculature, tumor sections were stained for CD31 (red) and desmin (green) as described above. 5 fields per tumor were randomly identified at original magnification ×200, and those blood vessels at least 50% covered by green desmin-positive cells were considered to be positive for pericyte coverage.

Plasma bFGF concentration analysis. bFGF levels were measured in the plasma of tumor-bearing animals by multiplex bead assay (BioRad and Millipore) in a 96-well plate according to the manufacturer's protocol. Concentrations were calculated based on a standard curve derived by performing 6 serial dilutions of a protein standard in assay diluent. Plasma samples were tested in duplicate, and the mean value was used for analysis.

Orthotopic lung adenocarcinoma model. Male 8-week-old athymic Ncr (*nu/nu*) mice were maintained in a specific pathogen–free mouse colony in accordance with regulations and standards of the Department of Agriculture and the Department of Health and Human Services. Mice were anesthetized with a combination of ketamine HCl (86 mg/kg) and xylazine (17 mg/kg) in normal saline; 100 μl solution per 10 g body weight was injected i.p. Mice were then placed in the right lateral decubitus position. The skin overlying the left chest wall in the midaxillary line was prepped with alcohol and incised (~7 mm), and the underlying chest wall was visualized. Logarithmically growing H441 cells (1×10^6 cells in single-cell suspensions of greater than 95% viability as determined by Trypan blue exclusion) in 50 μl HBSS containing 50 μg growth factor–reduced Matrigel (BD Bioscience) were injected into the left thorax at the lateral dorsal axillary line and into the left lung. After tumor cell inoculation, the skin incision was clipped, and the mice were turned to the left lateral decubitus position and observed until fully recovered. No anesthesia or surgery-related deaths occurred. 3 weeks after H441 tumor cell injection, 8 mice were euthanized for evaluation of baseline tumor volume ($n = 8$). Animals were sacrificed when moribund. Orthotopic tumors were photographed, and tissues were collected for IHC studies.

Alpha Innotech IF quantification. Alpha Innotech software (version 3.000) was used to quantify the IF signal in 5–10 random microscopic fields, depending on the tumor size, captured from at least 4 tumor specimens per group analyzed. Each microphotograph was collected using the same original magnification to obtain equal-sized images. 2 equally sized circles (area, 25,000 pixels) were randomly distributed on each microphotograph, and blue, red, and green pixel sums, averages, and background-corrected averages were obtained. The background-corrected fluorescent area of interest (green for p-EGFR, red for F4/80 and α-SMA) was normalized relative to the blue (nuclei) area for each analyzed microphotograph, and the mean ratio from all the images of each tumor specimen was calculated per treatment group.

Reagents, tumor cell lines, conditions, qRT-PCR, IHC, and LSC. See Supplemental Methods.

Statistics. Unless otherwise indicated, data are mean ± SEM. Distribution of PFS was estimated by the Kaplan-Meier method. Log-rank (Mantel-Cox) test was performed to test the difference in survival between groups. For comparison of continuous variables between 2 groups, 2-tailed Student's *t* test and Mann-Whitney-Wilcoxon test were used. A *P* value less than 0.05 was considered significant.

Acknowledgments

This study was supported in part by the Department of Defense BATTLE W81XWH-06-1-0303, Department of Defense PROSPECT award W81XWH-07-1-03060, University of Texas Southwestern Medical Center, University of Texas M.D. Anderson Cancer Center Lung SPORE NIH grant P50 CA070907 and NCI grant

P30CA016672, and research support from AstraZeneca. J.V. Heymach is a Damon Runyon-Lilly Clinical Investigator supported in part by Damon Runyon Cancer Research Foundation grant CI 24-04 and is also supported by the Physician Scientist Program at M.D. Anderson Cancer Center. We gratefully acknowledge Donna Reynolds (University of Texas M.D. Anderson Cancer Center) for providing us with cut tissue sections and helping with IHC protocols; Michael Worley (University of Texas M.D. Anderson Cancer Center) for editing the manuscript; Anderson Ryan, Juliane Jürgensmeier, and Lee Ellis for helpful scientific discussions; and AstraZeneca for providing vandetanib. Research in the laboratory of F. Ciardiello is supported by a grant from the Associazione Italiana per la Ricerca sul Cancro (AIRC).

Received for publication January 21, 2010, and accepted in revised form January 26, 2011.

Address correspondence to: John V. Heymach, Departments of Thoracic/Head and Neck Medical Oncology and Cancer Biology, University of Texas M.D. Anderson Cancer Center, Unit 432, 1515 Holcombe Blvd., Houston, Texas 77030, USA. Phone: 713.792.6363; Fax: 713.792.1220; E-mail: jheymach@mdanderson.org.

1. Folkman J, Shing Y. Angiogenesis. *J Biol Chem*. 1992;267(16):10931–10934.
2. Folkman J. Tumor angiogenesis: therapeutic implications. *N Engl J Med*. 1971;285(21):1182–1186.
3. Carmeliet P, Jain RK. Angiogenesis in cancer and other diseases. *Nature*. 2000;407(6801):249–257.
4. Ferrara N, Gerber HP, LeCouter J. The biology of VEGF and its receptors. *Nat Med*. 2003;9(6):669–676.
5. Ferrara N, Davis-Smyth T. The biology of vascular endothelial growth factor. *Endocr Rev*. 1997; 18(1):4–25.
6. Ellis LM, Hicklin DJ. VEGF-targeted therapy: mechanisms of anti-tumour activity. *Nat Rev Cancer*. 2008;8(8):579–591.
7. Kerbel RS. Tumor angiogenesis. *N Engl J Med*. 2008;358(19):2039–2049.
8. Jain RK, di Tomaso E, Duda DG, Loeffler JS, Sorensen AG, Batchelor TT. Angiogenesis in brain tumours. *Nat Rev Neurosci*. 2007;8(8):610–622.
9. Ferrara N, Hillan KJ, Gerber HP, Novotny W. Discovery and development of bevacizumab, an anti-VEGF antibody for treating cancer. *Nat Rev Drug Discov*. 2004;3(5):391–400.
10. Dvorak HF. Vascular permeability factor/vascular endothelial growth factor: a critical cytokine in tumor angiogenesis and a potential target for diagnosis and therapy. *J Clin Oncol*. 2002;20(21):4368–4380.
11. Chung AS, Lee J, Ferrara N. Targeting the tumour vasculature: insights from physiological angiogenesis. *Nat Rev Cancer*. 2010;10(7):505–514.
12. Sandler A, et al. Paclitaxel-carboplatin alone or with bevacizumab for non-small-cell lung cancer. *N Engl J Med*. 2006;355(24):2542–2550.
13. Hurwitz H, et al. Bevacizumab plus irinotecan, fluorouracil, and leucovorin for metastatic colorectal cancer. *N Engl J Med*. 2004;350(23):2335–2342.
14. Crawford Y, Ferrara N. Tumor and stromal pathways mediating refractoriness/resistance to anti-angiogenic therapies. *Trends Pharmacol Sci*. 2009;30(12):624–630.
15. Ebos JM, Lee CR, Kerbel RS. Tumor and host-mediated pathways of resistance and disease progression in response to antiangiogenic therapy. *Clin Cancer Res*. 2009;15(16):5020–5025.
16. Bergers G, Hanahan D. Modes of resistance to anti-angiogenic therapy. *Nat Rev Cancer*. 2008; 8(8):592–603.
17. Casanovas O, Hicklin DJ, Bergers G, Hanahan D. Drug resistance by evasion of antiangiogenic targeting of VEGF signaling in late-stage pancreatic islet tumors. *Cancer Cell*. 2005;8(4):299–309.
18. Graeber TG, et al. Hypoxia-mediated selection of cells with diminished apoptotic potential in solid tumours. *Nature*. 1996;379(6560):88–91.
19. Yu JL, Rak JW, Coomber BL, Hicklin DJ, Kerbel RS. Effect of p53 status on tumor response to antiangiogenic therapy. *Science*. 2002;295(5559):1526–1528.
20. Leenders WP, et al. Antiangiogenic therapy of cerebral melanoma metastases results in sustained tumor progression via vessel co-option. *Clin Cancer Res*. 2004;10(18 pt 1):6222–6230.
21. Davis DW, et al. Pharmacodynamic analysis of target inhibition and endothelial cell death in tumors treated with the vascular endothelial growth factor receptor antagonists SU5416 or SU6668. *Clin Cancer Res*. 2005;11(2 pt 1):678–689.
22. Heymach JV, et al. Phase II study of the antiangiogenic agent SU5416 in patients with advanced soft tissue sarcomas. *Clin Cancer Res*. 2004; 10(17):5732–5740.
23. Shojaei F, et al. Tumor refractoriness to anti-VEGF treatment is mediated by CD11b+Gr1+ myeloid cells. *Nat Biotechnol*. 2007;25(8):911–920.
24. Ferrara N. Role of myeloid cells in vascular endothelial growth factor-independent tumor angiogenesis. *Curr Opin Hematol*. 2010;17(3):219–224.
25. Crawford Y, et al. PDGF-C mediates the angiogenic and tumorigenic properties of fibroblasts associated with tumors refractory to anti-VEGF treatment. *Cancer Cell*. 2009;15(1):21–34.
26. Naumov GN, et al. Combined vascular endothelial growth factor receptor and epidermal growth factor receptor (EGFR) blockade inhibits tumor growth in xenograft models of EGFR inhibitor resistance. *Clin Cancer Res*. 2009;15(10):3484–3494.
27. Kobayashi S, et al. EGFR mutation and resistance of non-small-cell lung cancer to gefitinib. *N Engl J Med*. 2005;352(8):786–792.
28. Pao W, et al. KRAS mutations and primary resistance of lung adenocarcinomas to gefitinib or erlotinib. *PLoS Med*. 2005;2(1):e17.
29. Jain RK. Normalization of tumor vasculature: an emerging concept in antiangiogenic therapy. *Science*. 2005;307(5706):58–62.
30. Batchelor TT, et al. AZD2171, a pan-VEGF receptor tyrosine kinase inhibitor, normalizes tumor vasculature and alleviates edema in glioblastoma patients. *Cancer Cell*. 2007;11(1):83–95.
31. Greenberg JI, Cheresh DA. VEGF as an inhibitor of tumor vessel maturation: implications for cancer therapy. *Expert Opin Biol Ther*. 2009;9(11):1347–1356.
32. Jain RK. Normalizing tumor vasculature with anti-angiogenic therapy: A new paradigm for combination therapy. *Nat Med*. 2001;7(9):987–989.
33. Mukohara T, et al. Differential effects of gefitinib and cetuximab on non-small-cell lung cancers bearing epidermal growth factor receptor mutations. *J Natl Cancer Inst*. 2005;97(16):1185–1194.
34. Jacoby JJ, et al. Treatment with HIF-1alpha antagonist PX-478 inhibits progression and spread of orthotopic human small cell lung cancer and lung adenocarcinoma in mice. *J Thorac Oncol*. 2010;5(7):940–949.
35. Shojaei F, et al. G-CSF-initiated myeloid cell mobilization and angiogenesis mediate tumor refractoriness to anti-VEGF therapy in mouse models. *Proc Natl Acad Sci U S A*. 2009;106(16):6742–6747.
36. Shojaei F, Zhong C, Wu X, Yu L, Ferrara N. Role of myeloid cells in tumor angiogenesis and growth. *Trends Cell Biol*. 2008;18(8):372–378.
37. Boehm T, Folkman J, Browder T, O'Reilly MS. Antiangiogenic therapy of experimental cancer does not induce acquired drug resistance. *Nature*. 1997;390(6658):404–407.
38. Kerbel RS. Inhibition of tumor angiogenesis as a strategy to circumvent acquired resistance to anti-cancer therapeutic agents. *Bioessays*. 1991;13(1):31–36.
39. Heymach JV, et al. Randomized phase II study of vandetanib alone or with paclitaxel and carboplatin as first-line treatment for advanced non-small-cell lung cancer. *J Clin Oncol*. 2008;26(33):5407–5415.
40. Broxterman HJ, Lankelma J, Hoekman K. Resistance to cytotoxic and anti-angiogenic anticancer agents: similarities and differences. *Drug Resist Updat*. 2003;6(3):111–127.
41. Kerbel RS, et al. Possible mechanisms of acquired resistance to anti-angiogenic drugs: implications for the use of combination therapy approaches. *Cancer Metastasis Rev*. 2001;20(1–2):79–86.
42. Ellis LM, Hicklin DJ. Pathways mediating resistance to vascular endothelial growth factor-targeted therapy. *Clin Cancer Res*. 2008;14(20):6371–6375.
43. Heymach JV, Sledge GW, Jain RK. Tumor angiogenesis. In: Hong WK, et al., eds. *Holland–Frei Cancer Medicine 8*. Shelton, Connecticut, USA: People's Medical Publishing House–USA; 2010:149–169.
44. Ferrara N. Pathways mediating VEGF-independent tumor angiogenesis. *Cytokine Growth Factor Rev*. 2010;21(1):21–26.
45. Kopetz S, et al. Phase II trial of infusional fluorouracil, irinotecan, and bevacizumab for metastatic colorectal cancer: efficacy and circulating angiogenic biomarkers associated with therapeutic resistance. *J Clin Oncol*. 2010;28(3):453–459.
46. Iivanainen E, et al. The EGFR inhibitor gefitinib suppresses recruitment of pericytes and bone marrow-derived perivascular cells into tumor vessels. *Microvasc Res*. 2009;78(3):278–285.
47. Nolan-Stevaux O, et al. Differential contribution to neuroendocrine tumorigenesis of parallel Egfr signaling in cancer cells and pericytes. *Genes and Cancer*. 2010;1(2):125–141.
48. di Tomaso E, et al. PDGF-C induces maturation of blood vessels in a model of glioblastoma and attenuates the response to anti-VEGF treatment. *PLoS One*. 2009;4(4):e5123.
49. Greenberg JI, et al. A role for VEGF as a negative regulator of pericyte function and vessel maturation. *Nature*. 2008;456(7223):809–813.
50. Pietras K, Pahler J, Bergers G, Hanahan D. Functions of paracrine PDGF signaling in the proangiogenic tumor stroma revealed by pharmacological targeting. *PLoS Med*. 2008;5(1):e19.
51. Ostman A, Heldin CH. PDGF receptors as targets in tumor treatment. *Adv Cancer Res*. 2007;97:247–274.
52. Amin DN, Hida K, Bielenberg DR, Klagsbrun M. Tumor endothelial cells express epidermal growth factor receptor (EGFR) but not ErbB3 and are responsive to EGF and to EGFR kinase inhibitors. *Cancer Res*. 2006;66(4):2173–2180.
53. Cheng H, et al. Construction of a novel constitutively active chimeric EGFR to identify new targets for therapy. *Neoplasia*. 2005;7(12):1065–1072.
54. Wu W, et al. Expression of epidermal growth factor (EGF)/transforming growth factor-alpha by human lung cancer cells determines their response to EGF receptor tyrosine kinase inhibition in the lungs of mice. *Mol Cancer Ther*. 2007;6(10):2652–2663.
55. Kuwai T, et al. Phosphorylated epidermal growth factor receptor on tumor-associated endothelial cells is a primary target for therapy with tyrosine

kinase inhibitors. *Neoplasia*. 2008;10(5):489–500.
56. Kandel J, Bossy-Wetzel E, Radvanyi F, Klagsbrun M, Folkman J, Hanahan D. Neovascularization is associated with a switch to the export of bFGF in the multistep development of fibrosarcoma. *Cell*. 1991;66(6):1095–1104.
57. Paris F, et al. Endothelial apoptosis as the primary lesion initiating intestinal radiation damage in mice. *Science*. 2001;293(5528):293–297.
58. Karsan A, Yee E, Poirier GG, Zhou P, Craig R, Harlan JM. Fibroblast growth factor-2 inhibits endothelial cell apoptosis by Bcl-2-dependent and independent mechanisms. *Am J Pathol*. 1997;151(6):1775–1784.
59. Giatromanolaki A, et al. Relation of hypoxia inducible factor 1 alpha and 2 alpha in operable non-small cell lung cancer to angiogenic/molecular profile of tumours and survival. *Br J Cancer*. 2001; 85(6):881–890.
60. Semenza GL. Targeting HIF-1 for cancer therapy. *Nat Rev Cancer*. 2003;3(10):721–732.
61. Franco M, et al. Targeted anti-vascular endothelial growth factor receptor-2 therapy leads to short-term and long-term impairment of vascular function and increase in tumor hypoxia. *Cancer Res*. 2006; 66(7):3639–3648.
62. Roland CL, et al. Inhibition of vascular endothelial growth factor reduces angiogenesis and modulates immune cell infiltration of orthotopic breast cancer xenografts. *Mol Cancer Ther*. 2009;8(7):1761–1771.
63. Kim KJ, et al. Inhibition of vascular endothelial growth factor-induced angiogenesis suppresses tumour growth in vivo. *Nature*. 1993;362(6423):841–844.
64. Willett CG, et al. Direct evidence that the VEGF-specific antibody bevacizumab has antivascular effects in human rectal cancer. *Nat Med*. 2004;10(2):145–147.
65. Tong RT, Boucher Y, Kozin SV, Winkler F, Hicklin DJ, Jain RK. Vascular normalization by vascular endothelial growth factor receptor 2 blockade induces a pressure gradient across the vasculature and improves drug penetration in tumors. *Cancer Res*. 2004;64(11):3731–3736.
66. Lu C, et al. Impact of vessel maturation on anti-angiogenic therapy in ovarian cancer. *Am J Obstet Gynecol*. 2008;198(4):477.e1–477.e9.
67. Bergers G, Song S, Meyer-Morse N, Bergsland E, Hanahan D. Benefits of targeting both pericytes and endothelial cells in the tumor vasculature with kinase inhibitors. *J Clin Invest*. 2003;111(9):1287–1295.
68. Amin DN, Bielenberg DR, Lifshits E, Heymach JV, Klagsbrun M. Targeting EGFR activity in blood vessels is sufficient to inhibit tumor growth and is accompanied by an increase in VEGFR-2 dependence in tumor endothelial cells. *Microvasc Res*. 2008; 76(1):15–22.
69. Miller VA, O'Connor P, Soh C, Kabbinavar F. A randomized, double-blind, placebo-controlled, phase IIIb trial (ATLAS) comparing bevacizumab (B) therapy with or without erlotinib (E) after completion of chemotherapy with B for first-line treatment of locally advanced recurrent, or metastatic non-small cell lung cancer (NSCLC). *J Clin Oncol*. 2009;27(suppl):S18.
70. Kabbinavar FF, et al. Overall survival (OS) in ATLAS, a phase IIIb trial comparing bevacizumab (B) therapy with or without erlotinib (E) after completion of chemotherapy (chemo) with B for first-line treatment of locally advanced, recurrent, or metastatic non-small cell lung cancer (NSCLC). *J Clin Oncol*. 2010;28(suppl):Abstract 7526.
71. Natale RB, et al. Vandetanib versus gefitinib in patients with advanced non-small-cell lung cancer: results from a two-part, double-blind, randomized phase II study. *J Clin Oncol*. 2009;27(15):2523–2529.
72. Herbst RS, et al. Phase II study of efficacy and safety of bevacizumab in combination with chemotherapy or erlotinib compared with chemotherapy alone for treatment of recurrent or refractory non small-cell lung cancer. *J Clin Oncol*. 2007;25(30):4743–4750.
73. Hainsworth J, Herbst R. A phase III, multicenter, placebo-controlled, double-blind, randomized clinical trial to evaluate the efficacy of bevacizumab (Avastin) in combination with erlotinib (Tarceva) compared with erlotinib alone for treatment of advanced non-small cell lung cancer after failure of standard first-line chemotherapy (BETA). *J Thor Oncol*. 2008;3:S302.
74. Hecht JR, et al. A randomized phase IIIB trial of chemotherapy, bevacizumab, and panitumumab compared with chemotherapy and bevacizumab alone for metastatic colorectal cancer. *J Clin Oncol*. 2009;27(5):672–680.
75. Punt CJ, et al. Randomized phase III study of capecitabine, oxaliplatin, and bevacizumab with or without cetuximab in advanced colorectal cancer (ACC), the CAIRO2 study of the Dutch Colorectal Cancer Group (DCCG). *J Clin Oncol*. 2008; 26(suppl):180s.
76. Bao R, et al. Targeting heat shock protein 90 with CUDC-305 overcomes erlotinib resistance in non-small cell lung cancer. *Mol Cancer Ther*. 2009; 8(12):3296–3306.
77. Van den Eynden GG, et al. Differential expression of hypoxia and (lymph)angiogenesis-related genes at different metastatic sites in breast cancer. *Clin Exp Metastasis*. 2007;24(1):13–23.
78. Kuwai T, et al. Intratumoral heterogeneity for expression of tyrosine kinase growth factor receptors in human colon cancer surgical specimens and orthotopic tumors. *Am J Pathol*. 2008;172(2):358–366.
79. Weidner N, Semple JP, Welch WR, Folkman J. Tumor angiogenesis and metastasis--correlation in invasive breast carcinoma. *N Engl J Med*. 1991;324(1):1–8.
80. Stockmann C, et al. Deletion of vascular endothelial growth factor in myeloid cells accelerates tumorigenesis. *Nature*. 2008;456(7223):814–818.